PART 1
FUNDAMENTALS

Surface and Colloidal Chemical Aspects of Wet Cleaning

Srini Raghavan, Manish Keswani, and Nandini Venkataraman

Department of Materials Science & Engineering
The University of Arizona
Tucson, Arizona, USA

Abstract

Surface and colloidal chemicals aspects relevant to wet chemical cleaning and drying of semiconductor surfaces are reviewed. Specific areas discussed in this chapter include surface charging of metal oxide and nitride films, development of an electrical double layer, zeta potential of electrified interfaces and its effect on particulate contamination, adsorption of surfactants and metal ions on insulating surfaces, principles of surface tension gradient drying, and wetting and penetration of high aspect ratio features.

Key words: interfacial phenomena, wet cleaning, surface charging of metal oxide and nitride, electrical double layer, metal adsorption, high aspect ratio cleaning, surface tension gradient drying

1.1 Introduction to Surface Chemical Aspects of Cleaning

The fabrication of integrated circuits requires a myriad of liquid-based etching and cleaning processes that are followed by rinsing and drying steps. Interfacial phenomena such as wetting, spreading, adsorption, adhesion, and surface charge play a critical role in determining the feasibility and efficiency of a liquid-based process step. The objective of this chapter is to discuss the fundamental science of the key interfacial phenomena relevant to wafer etching, cleaning, and drying. Specific areas discussed in this chapter include:

1. Surface charging of materials in aqueous cleaning and rinsing solutions – understanding of the physical phenomena related to the adhesion and removal of particulate contaminants and metal ions.
2. High aspect ratio cleaning – understanding the physical limitations induced by surface wetting and capillary forces for processes that require liquid penetration into narrow features.

3. Drying methods – understanding the physics of creating a surface tension gradient at the water/vapor interface through interfacial adsorption.

The aforementioned concepts should be considered in unison to understand and explain cleaning processes and to control contamination. For example, to remove metallic and particulate contamination, the cleaning chemical must wet the surface, desorb, and preferably complex the metal ion and create a surface which bears a charge of the same sign as that on the contaminant particles to prevent re-deposition.

1.2   Chemistry of Solid-Water Interface

Successful removal of colloidal particles from surfaces requires an understanding of the repulsive and attractive forces between the particle and the surface. The repulsive forces arise mainly from the interaction of charged double layer at the particle/solution and the wafer/solution interface. The degree of surface hydroxylation and acid-base characteristics of these hydroxyl groups impact the charging of a surface. Sections 1.2.1 and 1.2.2 describe the surface charging of silicon dioxide and silicon nitride in aqueous media.

1.2.1   Surface Charging of Oxide Films in Aqueous Solutions

The surface of a semi-metal oxide film is terminated with hydroxyl (–OH) groups. A comprehensive discussion of hydroxylation of an oxide surface is provided by Yopps *et al.* [1]. The density of these hydroxyl groups is roughly two to three per square nm [2]. When this oxide surface is immersed in an aqueous solution, the hydroxyl groups react with H^+ and OH^- ions. These interactions are represented using the following equilibrium equations [3]:

$$MOH + H^+ \leftrightarrow MOH_2^+ \qquad K_1 \qquad\qquad (1.1)$$

$$MOH \leftrightarrow MO^- + H^+ \qquad K_2 \qquad\qquad (1.2)$$
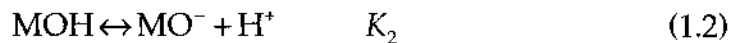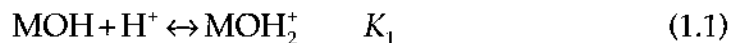
where M is a metal atom or an element such as Si.

Using the equilibrium constants (K_1 and K_2) for the reactions of the protonation (Eq. 1.1) and deprotonation (Eq. 1.2) of SiOH sites, the fraction of sites with positive, negative and zero charge, viz, θ_+, θ_- and θ_o on SiO_2 can be calculated as a function of solution pH. The result of such a calculation is shown in Figure 1.1 for SiO_2 using K_1 and K_2 values of $10^{0.7}$ and $10^{-3.9}$ respectively [4]. The surface charge density (coulombs per square meter), σ_{surf} at any particular pH is given by the expression:

$$\sigma_{surf} = N_s q(\theta_+ - \theta_-) \qquad\qquad (1.3)$$

where N_s represents the total number of surface sites per square meter, and q is the fundamental electronic charge (coulombs).
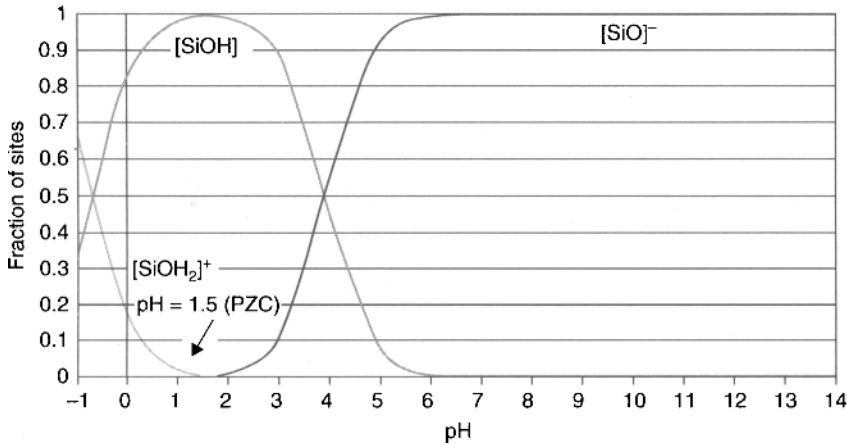
Figure 1.1. Fraction of positive, negative, and neutral sites on a SiO_2 surface immersed in water at various pH values calculated using $K_1 = 10^{0.7}$ and $K_2 = 10^{-3.9}$. Used with permission of the authors.

Figure 1.1 shows that the surface of SiO_2 is positively charged at low pH and negatively charged at high pH. At a pH of ~1.5, the fraction of positive sites is equal to the fraction of negative sites. This pH is called the point of zero charge (PZC) [5]. It is worth noting that at the PZC while the fractions of positively charged and negatively charged sites may be equal, each fraction may not be 0.5. The PZC value is roughly equal to the average of pK_1 and pK_2. Reference [6] outlines surface charging theory with respect to wafer cleaning.

Oxides may be classified as acidic, basic, or amphoteric [7]. Acidic oxides are generally oxides of non-metals (*e.g.* SiO_2, As_2O_3) that are dissolved by bases. By contrast, basic oxides (*e.g.* alkaline earth oxides such as MgO, FeO) are oxides of metals that are dissolved by acids. Oxides that show both acidic and basic properties are referred to as amphoteric oxides (*e.g.* Al_2O_3, SnO). Acidic oxides exhibit a low PZC while basic oxides exhibit higher PZC. For example, SiO_2, an acidic material, exhibits a PZC close to a pH of 2 while Al_2O_3, a basic material, exhibits a PZC close to a pH of 9. Table 1.1 lists PZC of materials of interest to semiconductor processing.

An acid- base mass titration technique is typically used to determine the PZC of materials. In this technique demonstrated by Schwarz, a suspension of oxide particles in an electrolyte is titrated with a standard acid/base solution [14]. The protonation/ deprotonation of the oxide surface causes the solution pH to increase/decrease from the original pH value. A mass balance from the added H^+/OH^- ions is then made to obtain the extent of adsorption of H^+ and OH^-. The surface charge density, σ_{surf} is given by:

$$\sigma_{surf} = F \times (\Gamma_{H^+} - \Gamma_{OH^-}) \tag{1.4}$$

where Γ_{H^+} and Γ_{OH^-} are adsorption densities (moles per square meter) of H^+ and OH^-, respectively, and F is the Faraday constant (96500 coulombs/gram equivalent).

The use of this technique is described in many papers [15–18] and only works well for samples with large surface areas such as particles. For materials with low surface areas such as oxide films, the pH change due to adsorption/desorption is too small to be accurately measured causing large errors in mass balance [19].

Table 1.1. Point of zero charge of materials of interest to wafer cleaning

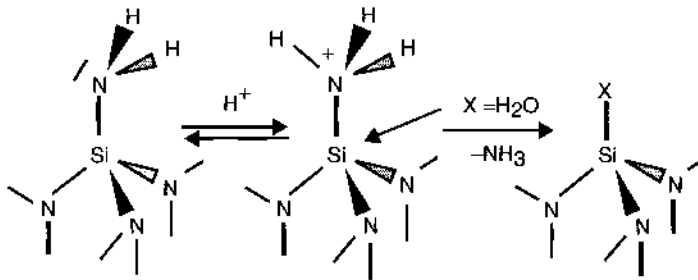| Material	PZC at pH of	Type	Reference
SiO_2	2–4	Acidic	[8] [9]
Si_3N_4	3–5.5	Depends on relative proportion of NH_2 and OH groups	[8] [9]
TiO_2	5–6	Weakly acidic	[10]
Al_2O_3	8–9	Amphoteric/mildly basic	[11] [12]
Si	3–4	Acidic	[8]
PSL	No PZC (negative charge at all pH values)	Not applicable (organic)	[13]

Figure 1.2. Charging of silicon nitride films in water; protonation of amine terminated surface sites leading to formation of positively charged sites that may react with water to form silanol groups [20]. Used with permission from Martin Knotter, NXP.

1.2.2 Surface Charging of Silicon Nitride Films in Aqueous Solutions

Silicon nitride films are most commonly deposited using a chemical vapor deposition (CVD) technique in which silane (SiH_4) reacts with ammonia (NH_3). Plasma-enhanced CVD (PECVD) forms SiN_x and low pressure CVD (LPCVD) forms Si_3N_4. Consequently, silicon nitride films may contain up to 5–6 atomic % hydrogen, especially those formed with PECVD. As shown in Figure 1.2, these films typically have amine (–NH_2) surface groups, which depending on their pK_a value can be protonated leading to the formation of positively charged sites [20]. The negative sites on the surface of nitride films have been postulated [21, 22] to be created by the reaction of surface amine groups with water forming silanol (Si-OH) followed by deprotonation to form negatively charged SiO⁻ sites. The isoelectric point (defined in Section 1.2.3) of nitride films can vary widely depending on the hydrolytic strength of –NH_2 groups, which in turn will depend on the solution pH, ionic strength, and temperature.

1.2.3 Electrified Interfaces: The Double Layer and Zeta Potential

A solid immersed in an aqueous solution produces a region of electrical inhomogeneity at the solid-solution interface. An excess charge at the solid-solution

interface is balanced by a diffuse region of equal but opposite charge on the liquid side. Composed of surface charge and its counter ions, this region is called the electrical double layer. Helmholtz was amongst the first to present a simple capacitor model for an electrical double layer [23]. Following this, a diffuse model of a double layer where the potential decreases exponentially from the surface into the bulk of the solution was put forth by Gouy and Chapman [24, 25]. Stern combined the capacitor model with the diffuse model and suggested that the double layer consists of two parts – an internal Stern layer and outer diffuse layer [26]. A more comprehensive review of recent theoretical models that seek to overcome the limitations of the Gouy-Chapman-Stern model is given in reference [27]. The following section provides a general discussion on selected phenomenological aspects of electrical double layers for oxide films that in principle can be applied to nitride films as well.

1.2.3.1   Oxide Films and Particles

The development of charge on the surface of oxides in contact with an aqueous solution results in an electrified interface. Hydrogen and hydroxyl ions that cause the development of surface charge are referred to as potential determining ions (PDI) [5] [28]. Figure 1.3 is a schematic sketch of the interface between SiO_2 and
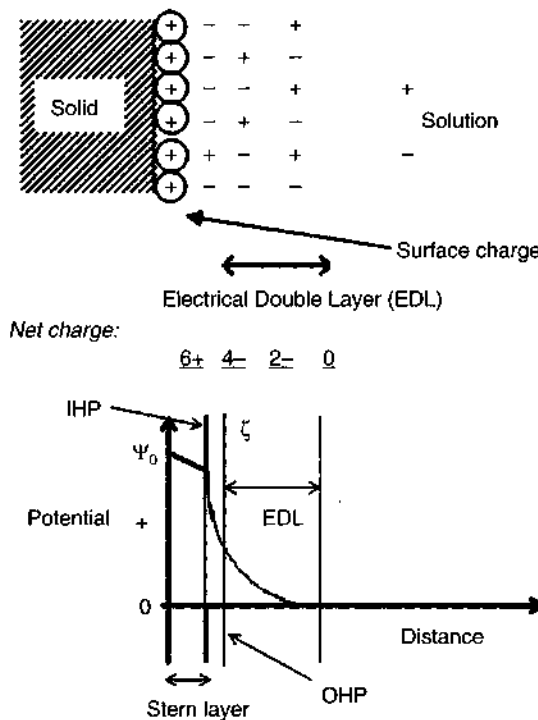

Figure 1.3. Schematic diagram of electrical double layer structure at the SiO_2/aqueous solution interface at a pH where the surface is positively charged. Used with permission from the authors.

H_2O at a pH value such that the surface has a positive charge. The six positive charges on the oxide surface are balanced by an equal number of negative charges in the surrounding liquid layers (net negative charges of 4 and 2 in the subsequent 1st and 2nd liquid layers from the surface) that line up close to the interface. Due to thermal motion of water molecules and ions, the charge balancing "counter ions" may be distributed in a few layers from the surface. The layer of positive charge and the "effective" layer of negative counter ions, shown in Figure 1.3, is referred to as the electrical double layer. This separation of charge at the interface leads to a surface potential, ψ_0. Experimentally it is not possible to measure ψ_0 for dielectric materials, but it can be calculated using a Nernst equation. For a metal immersed in a solution containing ions of its own kind, the classical Nernst equation is used for calculating the surface potential. However, if the potential determining ions are H^+ and OH^-, this equation converts to the following equation [28]:

$$\Psi_0 = \frac{\dfrac{RT}{F}\ln a_{H^+}}{(a_{H^+})_{PZC}} \tag{1.5}$$

where a_{H^+} is the activity of the hydrogen ion in the solution, $(a_{H^+})_{PZC}$ is the activity of the hydrogen ion at the pH value corresponding to point of zero charge (PZC) of the solid surface, F is the Faraday constant, and T is the temperature of the solution.

Rearranging Equation 1.5 and substituting the values of constants the following is obtained:

$$\psi_0(V) = 0.059(pH - PZC) \qquad \text{at } 25°C \tag{1.6}$$

According to Equation 1.6, the potential of an oxide surface should change by 59 mV at 25°C for a ten-fold change in H^+ ion concentration in solution. This same potential change is predicted by the classical Nernst equation (with H^+ replaced by the metal ion M^+) for a ten-fold change in univalent metal ion concentration.

The interfacial potential decreases from a value of ψ_0 on the surface to a value of zero in the bulk of the solution. The profile of potential decay with distance into the solution is schematically illustrated in the lower half of Figure 1.3. The profile of this decay has been discussed in many textbooks dealing with the electrical double layer phenomenon [29, 30]. The surface potential decays in a linear fashion from the surface to a location called the outer Helmholtz plane (OHP) which represents the closest distance of approach of electrostatically attracted counter ions. Beyond the OHP, the potential decays exponentially following a Boltzmann type distribution into solution. The potential of the double layer just outside the outer Helmholtz plane is known as zeta potential (ZP) indicated by ζ in Figure 1.3. Similar to the surface charge, ZP also varies with pH. The pH value at which the ZP of a material is zero is known as the isoelectric point (IEP) [28].

The zeta potential value depends on the profile of the decrease of the interfacial potential with distance from the surface. In solutions of high ionic strength, the surface charge is mostly balanced by counter ions in the OHP resulting in low values of ZP. For example, in a 1 M ionic strength solution, most of the potential drop would occur within a distance of 0.3 nm from the surface. This means that while the surface charge may be either positive or negative, ZP would be close to zero

in such solutions. In most of the cleaning solutions used in semiconductor manufacturing, such as SPM (sulfuric acid hydrogen peroxide mixture), BHF (buffered hydrofluoric acid), APM (ammonium hydroxide hydrogen peroxide mixture), and HPM (hydrochloric acid hydrogen peroxide mixture), the ionic strength is so high that the ZP of materials is likely to be close to zero. Because of this issue, cleaned wafers are typically re-immersed in dilute electrolyte solutions to measure the effect of cleaning treatments on the ZP of films. If the adsorption of ions causes the sign of zeta potential to be opposite to that of the surface charge, it is an indication that adsorption involves other forces in addition to electrostatic forces [5]. These ions, called specifically adsorbing ions, typically reside in the inner Helmholtz plane (IHP) and are much closer to the surface. For example, the adsorption of long chain cationic surfactants at an oxide/solution interface can change the ZP of a negatively charged surface from an initial negative value to a positive value [31].

The measurement of ZP is carried out using electrokinetic techniques. Two techniques are widely used for determining ZP during wafer cleaning. For colloidal particles, the technique of microelectrophoresis is used [29] [32]. In this technique, mobility of charged particles is measured in an applied electric field (e.g. using the Doppler effect). This mobility is then converted to ZP using Henry's equation given below [30].

$$\zeta = \frac{3\mu_E \eta}{2\varepsilon_r \varepsilon_0 f_1(\kappa a)} \tag{1.7}$$

where μ_E, ε_r, ε_0, η, κ and a are electrophoretic mobility, relative permittivity of solution, permittivity of vacuum, viscosity of solution, Debye-Huckel Parameter (inverse of Debye length), and radius of particle, respectively. The term $f_1(\kappa a)$ is a monotonically varying function that increases from 1.0 at $\kappa a = 0$ to 1.5 at $\kappa a = \infty$, in which case Equation 1.7 becomes the Smoluchowski equation.

The streaming potential technique is used for the ZP characterization of wafer surfaces [22]. Streaming potential arises when an ionic solution driven by a pressure gradient comes in contact with a charged stationary surface. When the solution flows, a part of the double layer charge is sheared and carried with the flowing solution giving rise to what is termed as streaming current. Streaming current/ potential is measured by placing two identical reversible electrodes at the two ends of the channel formed between two wafer surfaces [22, 33]. Zeta potential can be calculated from the gradient of measured streaming potential with respect to pressure drop across the channel using Equation 1.8 [30].

$$\zeta = \frac{\Delta E}{\Delta p} \frac{\eta K_e}{\varepsilon_r \varepsilon_0} \tag{1.8}$$

where ΔE and Δp are the potential difference and pressure drop across the two ends of a capillary/channel, and K_e is the electrolyte conductivity.

Using a streaming potential technique, there have been several reports of measurements of ZP of oxide, silicon, and nitride wafers [34, 35]. Strictly speaking, ZP exists only for surfaces that are insulating in nature. It is not meaningful to describe ZP for conductive metallic surfaces (e.g. gold particles, chromium coated quartz mask surface) without an insulating layer because charges are immediately
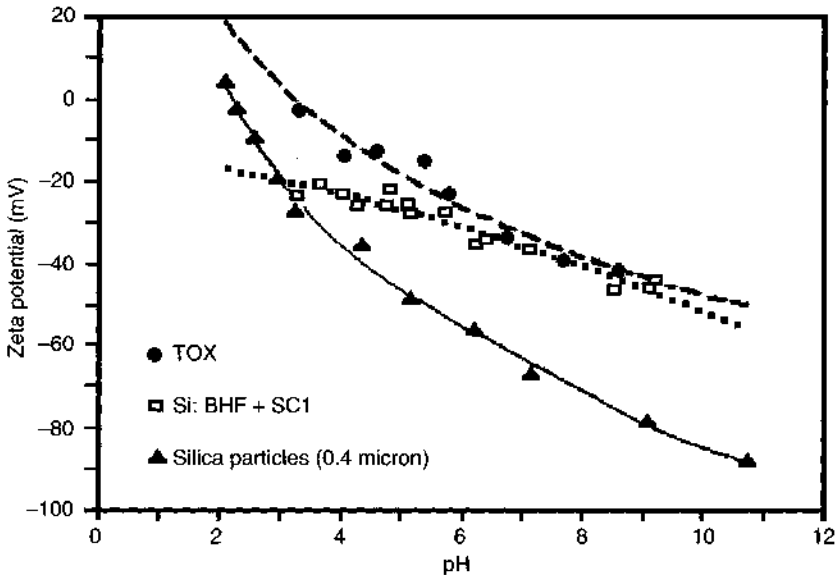
Figure 1.4. Comparison of zeta potential of silicon dioxide surfaces subjected to different surface treatments [33]. Used with permission of Raghunath Chilkunda.

conducted into the bulk of the metal. Data for ZP of metallic surfaces quoted in the literature could have only been obtained for metallic surfaces with an insulating surface layer [36, 37]. The zeta potentials of materials are known to be strongly dependent on surface preparation or synthesis procedure. For example, TiO_2 particles synthesized in a chloride-based medium may have a very different IEP than particles synthesized from a sulfate-based solution. An example of the effect of surface treatment on ZP of films is shown in Figure 1.4 [33]. In this figure, the measured ZP of thermal silicon dioxide (TOX) films and silicon subjected to BHF treatment followed by SC-1 (standard clean-1 or APM) leading to formation of a chemical oxide are shown. For comparison purposes, the ZP of colloidal silica particles (0.4 µm) is also shown. It may be discerned that the TOX films have an isoelectric point (IEP) close to a pH of 4 whereas colloidal silica particles have an IEP close to pH of 3. However, silicon coated with a chemical oxide film formed in the SC-1 solution does not exhibit an IEP in the pH range of 2 to 10 [33]. Even though all the films have a negative ZP in the pH range of 5 to 10, the value of IEP is dependent on the type of surface treatment.

1.2.3.2   Nitride Films and Particles

As in the case of oxide surfaces, the IEP of nitride surfaces is also sensitive to preparation procedures. Results from a study investigating the effect of different pretreatments on the IEP of nitride films is shown in Figure 1.5 [22]. Removal of surface oxide by BHF treatment yields a film with an IEP of approximately 5.3. Oxidizing pretreatments such as SPM and APM shift the isoelectric point to lower pH values. Silicon nitride particles are commonly used as model contaminant particles in wafer cleaning studies. The IEP of silicon nitride particles is a strong function of the method of preparation and the aging process, and thus can vary from a pH of 2.5 to 6.2 [38, 39].
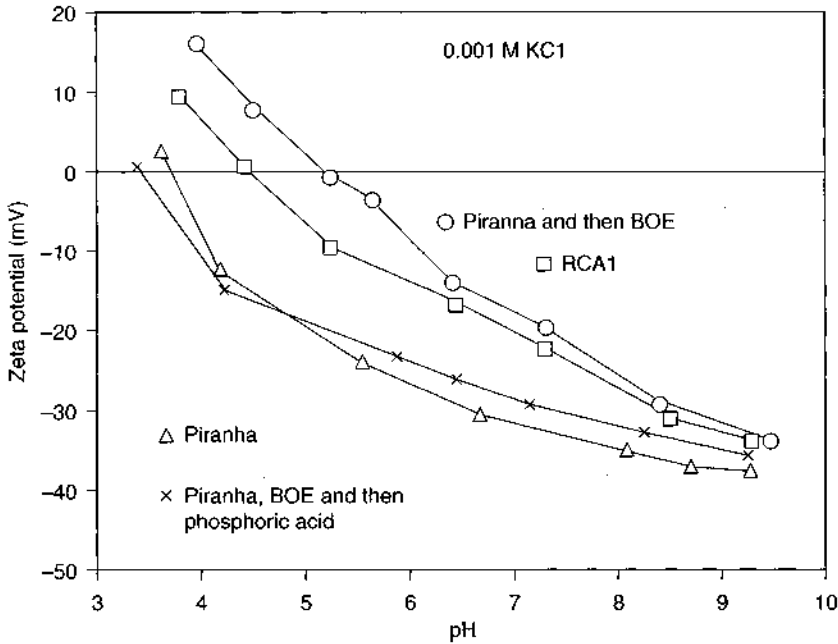
Figure 1.5. Effect of different surface treatments on the zeta potential of LPCVD silicon nitride films measured by streaming potential method [22]. Reproduced with permission of ECS – The Electrochemical Society from Jan, D. and Raghavan, S., *Journal of the Electrochemical Society*.

1.3   Particulate Contamination: Theory and Measurements

1.3.1   Effect of Electric Double Layer Formation on Particulate Contamination

The electric charge developed by particles affects contamination of the wafer surfaces during cleaning. If the charges on the contaminant particles and the wafer surface in a given liquid medium are opposite in sign, then electrostatic attraction between the particle and the surface is favorable. In the DLVO (Derjaguin and Landau, Verwey, and Overbeek) theory [40–42], the potential energy of interaction between two materials is considered to consist of two components, namely van der Waals and electrical double layer. The van der Waals (VDW) interaction energy, E_{VDW} is almost always attractive, and for the interaction between a spherical particle and a flat plate, it is given by the following equation:

$$E_{VDW} = -\frac{A_{132} \cdot a}{6D} \tag{1.9}$$

In Equation 1.9, A_{132} is the effective Hamaker constant between particle 1 and surface 2 immersed in medium 3, a is the radius of particle, and D is the closest distance of separation between particle and surface. The negative sign indicates that VDW interaction energy is attractive. The effective Hamaker constant between particle 1 and surface 2 immersed in a medium 3 can be calculated from the individual Hamaker constants of the three materials, A_{11}, A_{22}, and A_{33}, according to the following equation.

$$A_{132} = \left(\sqrt{A_{11}} - \sqrt{A_{33}}\right)\left(\sqrt{A_{22}} - \sqrt{A_{33}}\right) \tag{1.10}$$

The Hamaker constant of materials lies in the range of 10^{-19} to 10^{-20} J.

The electrostatic energy of interaction between the particle and the surface depends on the surface potential of the particle and the wafer (ψ_{01} and ψ_{02}, respectively), the closest distance of separation between the surface of the particle and the wafer (D), diameter of the particle (d), and the Debye length (κ) in the liquid medium. The Debye length is a function of the ionic strength of the medium and is given by:

$$\kappa = \left[\frac{1000q^2 N_A}{\varepsilon_r \varepsilon_0 k_B T} \sum_i z_i^2 M_i \right]^{0.5} \tag{1.11}$$

where q is the fundamental electronic charge, N_A is Avogadro's number, k_B is the Boltzmann constant, T is the absolute temperature, z_i is the charge on the ith ion, M_i is the molar concentration of ith ion, ε_0 is the permittivity of free space, and ε_r is the relative permittivity of the material with respect to vacuum. For surface potential values less than 50 mV, the expression for electrostatic interaction energy, E_{EDL} is given by:

$$E_{EDL} = \pi \varepsilon d \left(\Psi_{01}^2 + \Psi_{02}^2 \right) \left\{ \frac{2\Psi_{01}\Psi_{02}}{\Psi_{01}^2 + \Psi_{02}^2} \ln \frac{1 + e^{-\kappa D}}{1 - e^{-\kappa D}} + \ln \left[1 - e^{-2\kappa D} \right] \right\} \tag{1.12}$$

Replacement of surface potential by zeta potential in the above equation introduces minimal error if the surface potential values are small (<50 mV).

Several key comments may be made about this expression:

1. The electrostatic energy of interaction is proportional to the product of the surface potential of materials 1 and 2. Consequently, if the surface and the particle have surface potentials of the same sign, the electrostatic interaction energy will be positive or repulsive. Alternatively, if the surface or zeta potentials are of opposite signs, E_{EDL} will be negative or attractive.
2. Higher ionic strength solutions result in larger values of k that will significantly reduce the magnitude of E_{EDL}. For a very large value of k, E_{EDL} will be close to zero.
3. In low dielectric constant solutions such as organic liquids, E_{EDL} will be quite small.

Figure 1.6 is a schematic illustration of van der Waals interaction energy, electrostatic interaction energy and sum of the two components as a function of distance of separation between a particle and a surface. In the figure, attractive energy is denoted by a negative sign whereas repulsive energy is denoted by a positive sign. As may be seen, the total energy of interaction exhibits a maximum at a certain distance from the surface. This maximum represents a barrier for particle deposition on the surface. The height of the barrier would decrease with an increase in ionic strength of the solution. Reduction in barrier height would favor particle deposition.

The importance of ionic strength of solutions on particle contamination was elegantly demonstrated by Riley and Carbonell using silica particles [43]. They investigated the contamination of cleaned silicon wafers in solutions of different ionic
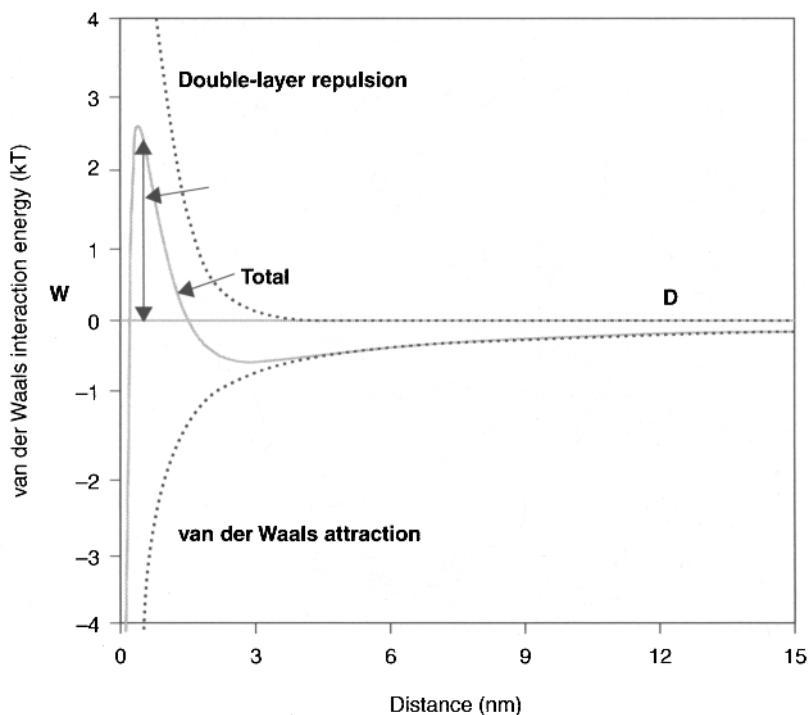
Figure 1.6. Schematic plots of van der Waals interaction energy, electrostatic interaction energy, and the sum of the two energies against distance of separation between a particle and a surface. Used with permission from the authors.

strength containing mono-sized silica particles at pH values where the zeta potential of wafer and particles are both negative. The results of their study are plotted as normalized surface coverage as a function of ionic strength in Figure 1.7. Normalized surface coverage is defined as the ratio of the number of particles deposited on wafers submerged into contaminated solution for 5 min to that deposited on wafers dipped for a few seconds. The results indicate that particle deposition on wafers increases sharply at an electrolyte concentration of 0.01 M. The κ value at this electrolyte concentration is reasonably large (0.33 nm^{-1}); consequently, the electrostatic repulsion between particle and wafer is significantly reduced. Sulfuric acid hydrogen peroxide mixture, HPM, and BHF solutions have ionic strengths in excess of 1 M and, thus, provide conditions conducive to particulate contamination. Even though the ionic strength of 5:1:1 (H_2O:H_2O_2:NH_4OH) SC-1 solution is in excess of 1 M, deposited particles, if any, are continuously removed due to silicon etching [44].

1.3.2 Direct Measurement of Interaction Forces between Particles and Surfaces

Atomic force microscopy (AFM) has emerged as a very useful tool for directly measuring interaction forces between surfaces in air and liquid media [45]. A technique known as the colloidal probe method has been developed to measure interaction forces between particles and surfaces [45–47] and reviewed in [6]. In this technique, a single particle (1–50 μm) is attached to the end of an AFM
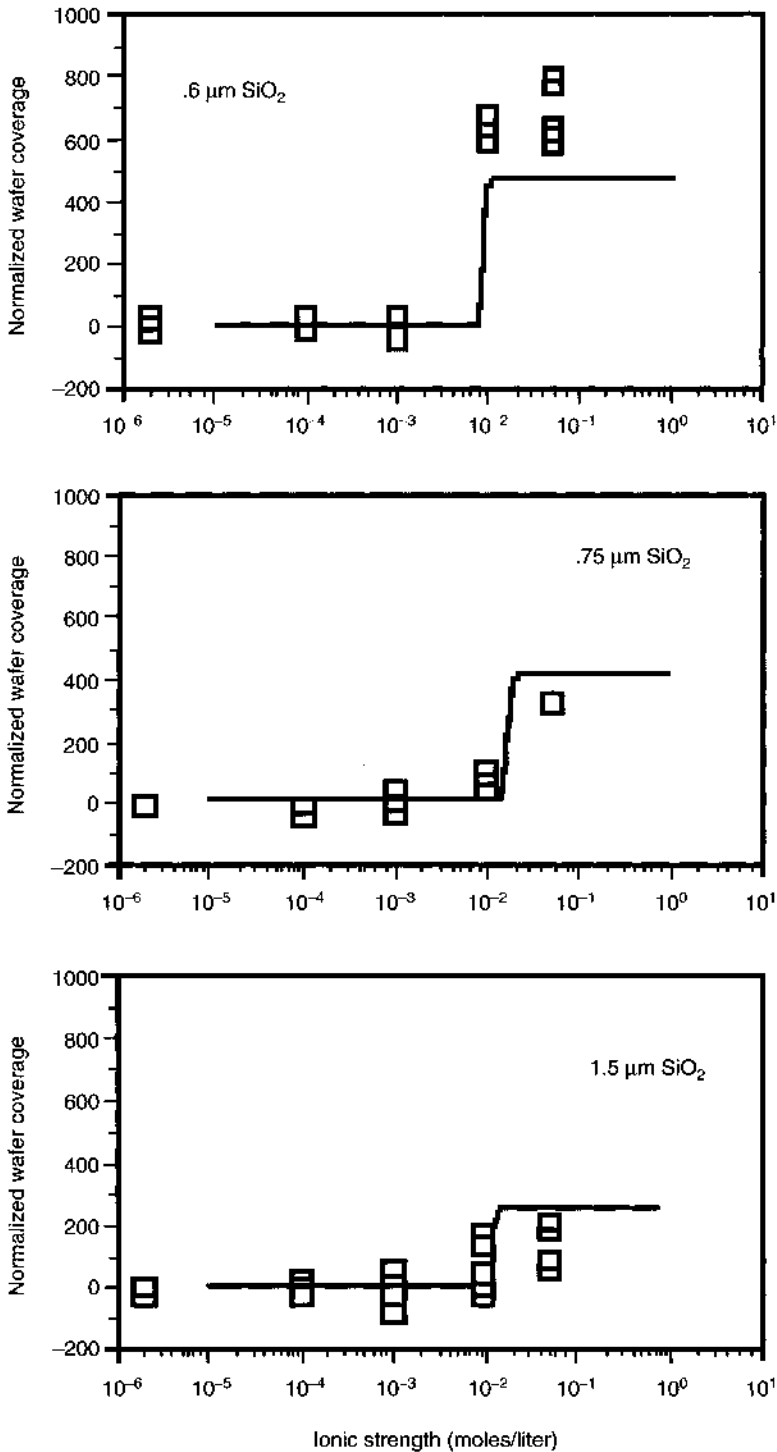
Figure 1.7. Normalized coverage of silicon wafers by 0.6, 0.75, and 1.5-μm sized silica particles as a function of ionic strength of solution [43]. Reprinted from *Journal of Colloid and Interface Science*, 158(2), Riley, D. J and Carbonell, R. G., "Mechanisms of Particle Deposition from Ultrapure Chemicals onto Semiconductor Wafers: Deposition from Bulk Liquid during Wafer Submersion", page 259. Copyright (1993) with permission from Elsevier.

cantilever, and the instrument measures the interaction forces during the particle approach towards and retraction from a surface. The adhesion can be quantified from the force measured during retraction.

An example of the measured force between a silicon dioxide surface and a silica particle (5 μm) in deionized water (DIW) is shown in Figure 1.8. A long-range repulsive force is observed starting at a separation distance of 40 nm. This repulsive force is due to the interaction between the electrical double layers on the negatively charged surfaces. The magnitude of the repulsive electrical double layer force continues to increase as the tip and the surface approach each other. When the tip-cantilever assembly is retracted from the surface, the force-distance curve closely follows the curve obtained during approach.

The interaction force between a hydrogen terminated silicon surface and hydrogen terminated silicon tip as a function of separation distance after time of immersion of 2, 10 and 60 min is shown in Figure 1.9. In this case, during approach (Figure 1.9a) only attractive forces exist between the surface and the tip after 2 and 10 min. The tip jump onto Si surface occurs at distances of 4.9 and 2.8 nm after 2 and 10 min, respectively, as indicated by down arrows. When the immersion time was increased to 60 min, a weak repulsive force was measured starting at a distance of ~ 15 nm. However, ultimately the force becomes attractive and the tip suddenly jumps onto the surface at a distance of ~ 2.0 nm. It has been reported in literature that the hydrogen terminated surface requires hours of immersion in aerated water to be transformed to a hydrophilic state. Therefore, it can be expected that the hydrophobic Si-H sites are not likely to be replaced by hydrophilic Si-OH sites after 2 and 10 min of immersion times. Therefore, only attractive forces were
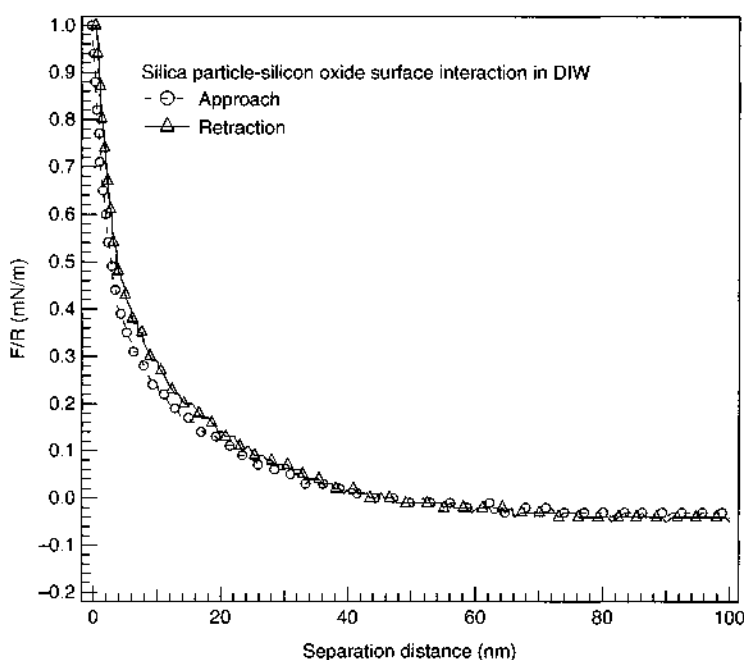

Figure 1.8. Normalized force as a function of separation distance between a silica particle and silicon oxide surface in DIW. Used with permission from the authors.
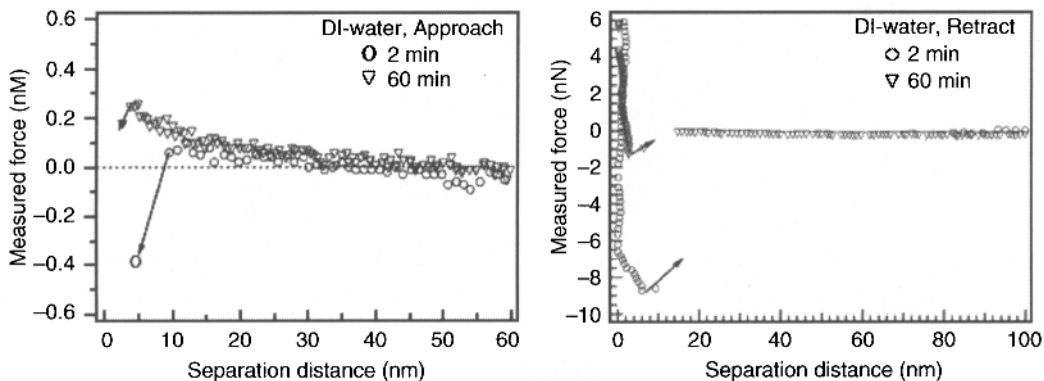
Figure 1.9. Force measured as a function of separation distance for interaction between a hydrophobic silicon tip and hydrophobic silicon surface in DIW: a) approach curve and b) retraction curve. Used with permission from the authors.

measured during approach between the silicon surface and the silicon tip. After 60 min of immersion time, the native oxide film that is formed would acquire a negative charge by dissociation of silanol groups (Si-OH) to SiO⁻ and H⁺. The measured repulsive force is a consequence of the establishment of negative charges of the surface and the tip.

The adhesion forces between silicon surface and silicon tip in DI-water can be measured from the retraction curves as shown in Figure 1.9b. It can be seen from this figure that a strong adhesion force of 10.5 nN exists after a short immersion time of 2 min. The results also show that as the immersion time increased from 2 to 10 and 60 min, the adhesion force decreased from 10.5 nN to 3.0 nN and 1.2 nN, respectively.

In an effort to understand particle deposition on silicon after processing in HF solutions, Chen and Singh [45] measured interaction forces between a HF-cleaned silicon nitride tip (representing nitride particles commonly used for contamination experiments) and a hydrogen terminated silicon surface in an acidic solution at pH = 1.88. The solution contained 0.1 wt% HF to prevent oxidation of surfaces. The results shown in Figure 1.10 reveal attraction between surfaces during approach as well as retraction indicating the dominant role of van der Waals forces. Addition of an anionic surfactant at ~1 wt% eliminated this attractive force.

Cooper *et al.* measured interaction forces between polystyrene latex (PSL) particles (5 μm) and silicon dioxide (SiO_2) surfaces in 0.03 M KNO_3 solution with pH ranging from 2 to 10 [48]. The results show a strong effect of pH on the force between the particle and the surface. A strong adhesion force of 127 nN was measured in an acidic solution with a pH of 3. This adhesion force is attributed to the van der Waals force that exists between the particle and the surface. Force measurements at a pH greater than 5 show a significant decrease in adhesion force ranging from 0 to 12 nN, as shown in Figure 1.11. Increasing the pH of the solution also resulted in a higher surface roughness due to etching of the oxide film in a basic solution. It was concluded that this increase in surface roughness causes the particle to interact mainly with the asperities and not the flat surface beneath, thereby reducing the interaction volume between particle and substrate. This results in the decrease of adhesion force between two surfaces. The measured adhesion force was compared with theoretically calculated forces using an adhesion force model that models
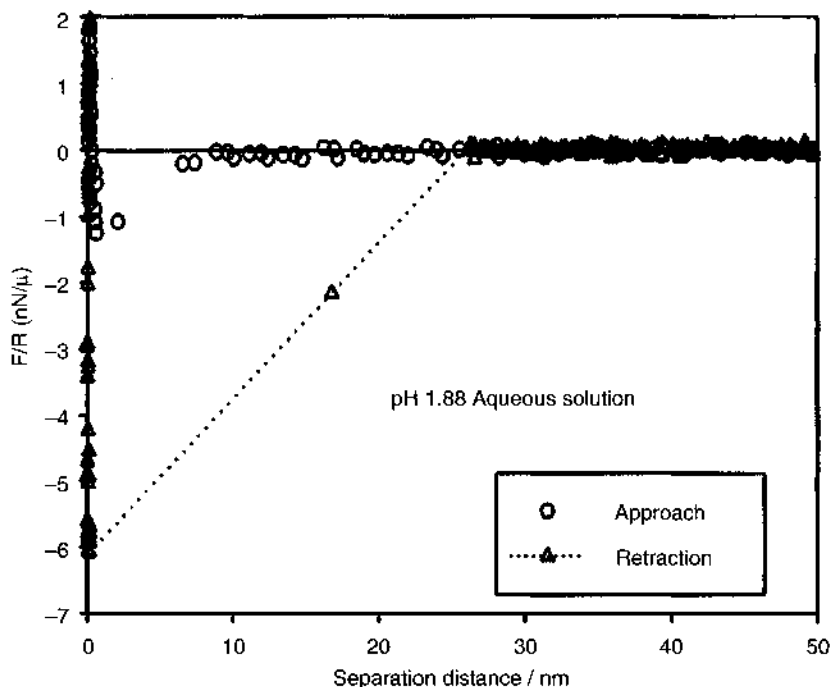
Figure 1.10. The normalized force as a function of separation distance between a silicon nitride tip and a silicon surface in an aqueous solution of pH 1.88 containing 0.1 wt% HF [45]. Reproduced with permission of ECS – The Electrochemical Society from Chen, Z. and Singh, R. K., *Journal of the Electrochemical Society*.

hemispherical asperities to represent surface roughness. Theoretically calculated adhesion force correlated well with experimentally measured force between PSL particles and SiO_2 surface in both acidic and basic solutions.

1.4   Influence of Surface Electrical Charges on Metal Ion Adsorption

Metal ion contamination on silicon oxide or nitride wafers typically occurs by adsorption and/or ion exchange. The extent of contamination is affected by charges developed on the surfaces and the nature of the metal ions (*i.e.* bare, hydrolyzed, cationic, anionic).

The adsorption of metal ions from solutions onto oxide and nitride films causes metallic contamination during wafer processing. According to Loewenstein et al., the adsorption of metal ions on silicon or silicon dioxide occurs by replacement of a hydrogen ion from a hydroxyl group by a metal ion [49]. The adsorption of metal ions can be modeled using basic surface chemical principles [50]. In order to elucidate the adsorption of metal ions onto oxides, it is very important to understand the aqueous chemistry of metal ions in solutions at different pH values. Multivalent bare metal ions such as Cu^{+2} and Fe^{+3} do not exhibit a tendency for adsorption, but the hydrolyzed forms (*e.g.* $Cu_2(OH)_2^{+2}$, $Cu(OH)^+$, $Cu(OH)_2$, $Cu(OH)^{-3}$, $Cu(OH)_4^{-2}$) adsorb strongly at the oxide/water interface. Hence aqueous speciation calculations are critical for modeling metal ion adsorption [51, 52].
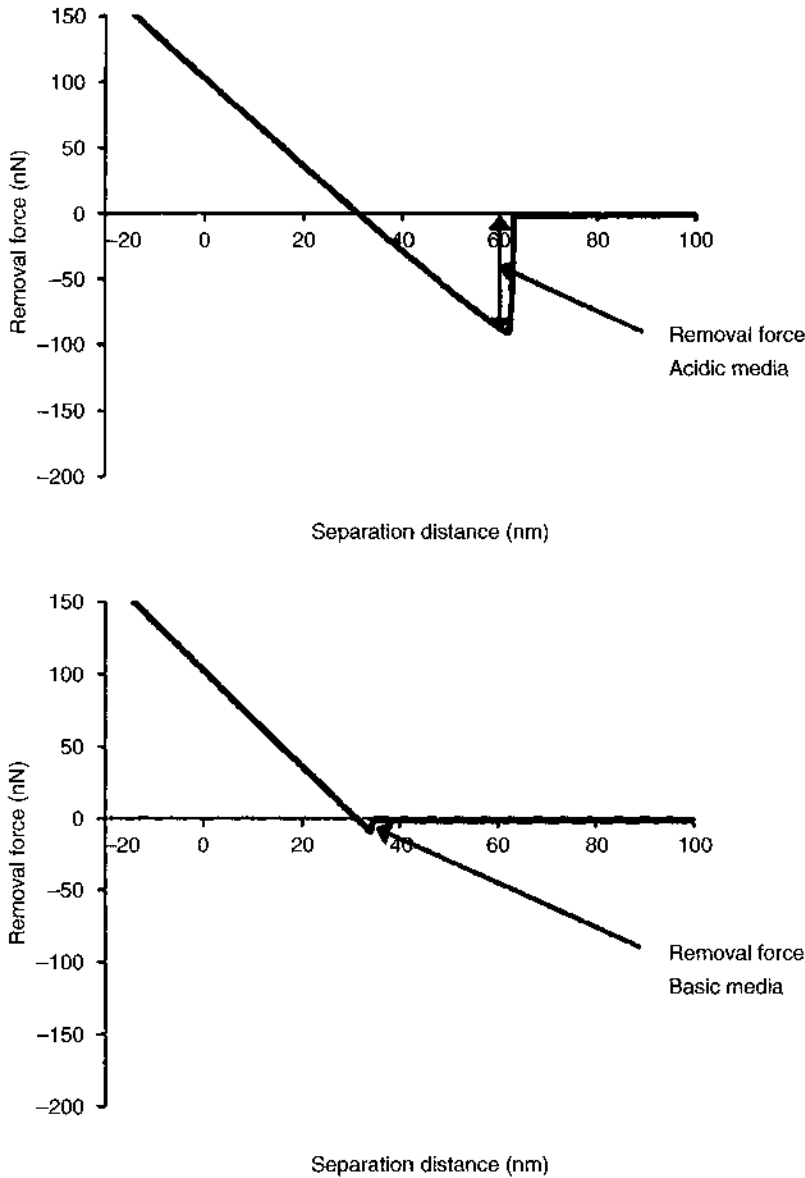
Figure 1.11. Interaction forces measured between a polystyrene latex particle and a silicon oxide surface. The upper curve represents the force *vs.* distance curve under acidic conditions. The lower curve is for the same system under basic conditions [48]. Reprinted from *Journal of Colloid and Interface Science*, 228(2), Cooper, K., Gupta A., and Beaudoin, S., "*Substrate Morphology and Particle Adhesion in Reacting Systems*", page 213. Copyright (2000) with permission from Elsevier.

An example of a speciation calculation using commercially available software [53] to obtain the total copper concentration of a 10-ppb solution, is shown in Figure 1.12a. At pH values less than 6, copper is predominantly in the form of the cupric cation (Cu^{+2}). Around pH of 6, copper ions begin to hydrolyze and, in the pH range 6–8, they predominantly exist as singly charged $CuOH^+$ and neutral $Cu(OH)_2$ species. The precipitation of insoluble CuO begins to occur at a pH of 7.5. In the pH range 8–10, 70% of copper is likely to be insoluble CuO and 30% as soluble $Cu(OH)_2$
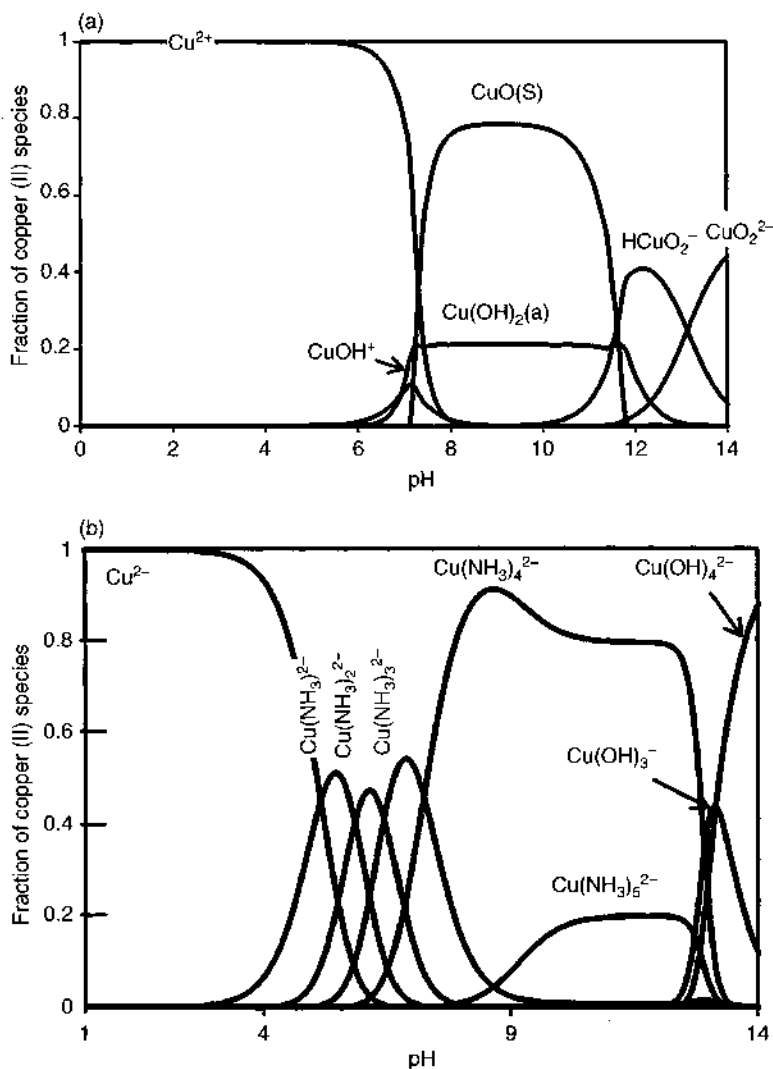
Figure 1.12. Speciation of copper in an aqueous solution a) without and b) with 1 M total ammonia, as a function of pH, for a total copper concentration of 10 ppb. Used with permission from the authors.

species. At alkaline values above pH of 11, the copper oxide begins to redissolve forming anionic copper hydroxide species.

The presence of complexing species such as NH_3 (i.e., in APM solution) can greatly alter the speciation. Figure 1.12b shows the results of speciation calculations carried out for an aqueous solution containing 10-ppb copper and 1 M ammonia. In the presence of ammonia, a number of soluble $Cu-NH_3$ complexes form. At pH values between 9 and 13, $Cu(NH_3)_4^{+2}$ is the predominant species. Ammonium hydroxide/hydrogen peroxide solutions typically have a pH of ~11 and can induce adsorption of copper in the form of $Cu(NH_3)_4^{+2}$ on a negatively charged chemical silicon oxide film. Similar speciation diagrams for Cu(I) and Cu(II) in ammonium chloride solutions predict the formation of $Cu(NH_3)_3Cl^+$, $Cu(NH_3)_4^{+2}$ and $Cu(NH_3)_5^{+2}$ complexes in alkaline solutions [54].

The adsorption of metal ions can occur by an ion exchange mechanism where the metal ions exchange with hydrogen ions in the surface hydroxyl groups. For adsorption of a metal ion M^+ on SiO_2, the exchange process can be represented as follows:

$$SiOH(s)+M^+(aq) \leftrightarrow SiOM(s)+H^+(aq) \qquad (1.13)$$
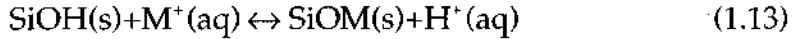
The equilibrium constant for the reaction, K_{exc}, can be written as:

$$K_{exc} = \frac{\theta_M [H^+]}{\theta_0 [M^+]} \qquad (1.14)$$

where θ_M is the fraction of surface sites occupied by the metal ion and θ_0 is the fraction of surface sites in the neutral hydroxylated form. Since the sum of θ_0 and θ_M equals one, the above equation can be rearranged to:

$$\theta_M = \frac{K_{exc}[M^+]}{[H^+]+K_{exc}[M^+]} \qquad (1.15)$$

If the initial number density (number/m^2) of hydroxyl groups is denoted as N, then the surface concentration of metal ions, σ_m, is:

$$\sigma_M = N\theta_M \qquad (1.16)$$

Using literature K_{exc} values for the interaction of copper ions with silica gels, Lee et al., have modeled the copper ion uptake by chemical silicon oxide wafers at different pH values [55]. The researchers also carried out calculations for copper using ion exchange data for SiOH groups given in Table 1.2. It may be noted that copper can bind with the –SiOH groups to form 1:1 ($SiOCu^+$) or 1:2 (($SiO)_2Cu$) surface species (complexes). The results obtained for a solution with copper ion

Table 1.2. Equilibrium data for ion exchange reactions involving SiOH groups and Cu^{+2} [55]. Used with permission from Material Research Society, reprinted from Lee, W., Torek, K. J., Palsulich, D. A., and Weston, L., *Science and Technology of Semiconductor Surface Preparation*, *Mat. Res. Soc. Symp. Proc.*, Volume 477(1977) page 57.

Equilibrium reaction	Log k
$SiOH + H^+ \rightarrow SiOH_2^+$	0.7
$SiOH \rightarrow SiO^- + H^+$	–3.9
$SiOH + Cu^{+2} \rightarrow SiOCu^+ + H^+$	–5.52
$2\,SiOH + Cu^{+2} \rightarrow (SiO)_2Cu + 2H^+$	–11.19

concentration of 10 ppb are shown in Figure 1.13. The results of the computation show:

1. The highest level of copper uptake occurs in the pH range of ~ 5.5 to ~9.5.
2. In the same pH range, the (surface) concentration of copper occupied sites is very small compared to the concentration of negative sites.

In two seminal papers, James and Healy provided excellent discussions of the adsorption of hydrolyzable metal ions on oxide surfaces [56, 57]. They measured the adsorption behavior of cations (Ca^{+2}, Co^{+2}, Fe^{+3}, La^{+3} and Th^{+4}) on silica. The effects of the adsorbed ions on the zeta potential of silica were also determined. For each metal ion, there was a critical pH where adsorption increased steeply over a very narrow pH range. This critical pH is usually just below the pH of the formation of bulk hydrolysis products. In the case of some metal ions, three isoelectric points were measured.

A multicomponent Langmuir model has been used to model competitive adsorption of metal ions and hydrogen ions onto oxidized silicon surfaces [49]. Representing the interaction constant of ions of type 'i' by K_i, the fraction of surface covered by ions of type 'i' is given by:

$$\theta_i = \frac{K_i[M^{i+}]}{1 + \Sigma_i K_i[M^{i+}]} \tag{1.17}$$

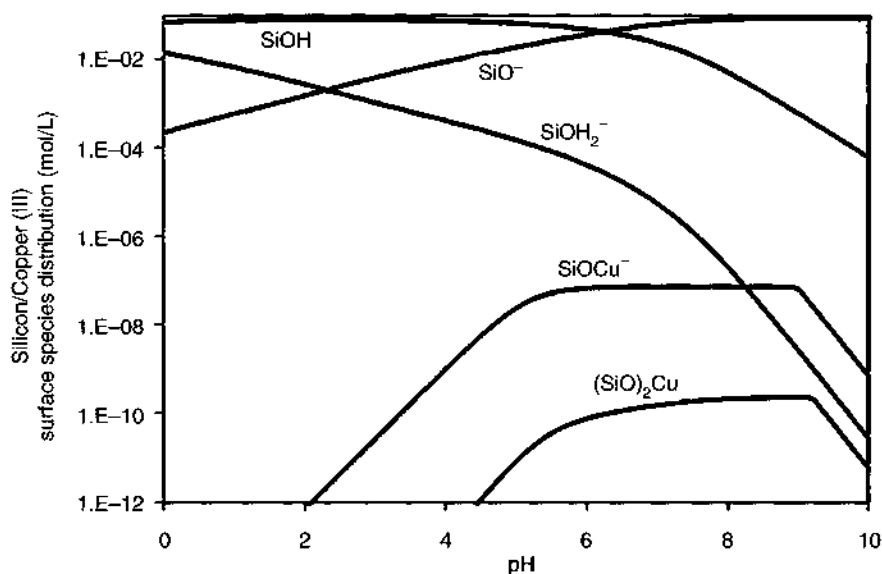**Figure 1.13.** Distribution of surface species as a function of pH when copper adsorbs on silica. For [Cu] = 10 ppb, SiO_2 = 1 M, surface area = 9613 cm² and 0.0871 M surface sites. Used with permission from the authors.

Unfortunately, pH-dependent speciation of the adsorbing metal ions has not been considered in this work. As pointed out earlier, hydrolysis of metal ions is pH dependent, and hydrolyzed metal ions exhibit much stronger adsorption on surfaces.

1.5   Wettability of Surfaces

1.5.1   Surface Tension and Surface Energy

Films that are cleaned and dried may be either high energy surfaces such as oxides, nitrides, and metals or low energy surfaces such as hydrogen terminated silicon, photoresists, and low-κ (low dielectric constant) materials or a combination of both types of surfaces. In some unique situations such as the etching of silicon by hydrofluoric acid, the high energy surface of silicon could be rendered into a low energy surface by hydrogen termination. Most liquid chemical formulations used in wet processing are aqueous solutions with surface tension of less than 72 mN/m (water has a surface tension of 73 mN/m [dyne/cm] at 20°C). However, buffered hydrogen fluoride solutions may have surface tension as high as 90 mN/m. Since more than one type of film may be exposed during a cleaning step, chemical formulations must be tailored to wet all of the surfaces that are involved. One of the film characteristics that aids in the choice of chemical formulations is the critical surface tension of wetting, γ_c. Liquid chemicals that have a surface tension equal to or less than γ_c will completely wet the solid. The determination of γ_c is typically done by the Zisman method [58]. In this method, contact angle (θ) of liquids or liquid mixtures of different surface tension on the surface of interest are measured, and a plot of cos θ versus surface tension is made. The surface tension of the liquid that gives a value of 1 for cos θ is designated as the γ_c of that surface.

The critical surface tension of wetting of an HF-etched silicon surface has been reported [59]. In this study, methanol/water solutions of different compositions containing 1 wt% HF with surface tensions in the range of 72–23 mN/m were used, and the surface tension results are shown in Figure 1.14. Using the Zisman method, the critical surface tension of wetting has been determined to be approximately 27 mN/m.

1.5.2   Adsorption Characteristics and Wettability Modification

Surface active agents or surfactants are added to cleaning formulations for a variety of reasons including reduction of surface tension for modification of wettability of surfaces, and prevention of particle deposition as well as plating of metal ions. Typically, these agents are organic chemicals with a hydrophobic tail and a hydrophilic head. For surfactants that are used in wafer cleaning, the hydrophobic part of the molecule typically contains alkyl and/or phenol groups along with hydrophilic groups such as polyethylene oxide or polyglycidol to control the hydrophilic-lipophilic balance (HLB). The hydrophilic head is either a neutral hydroxyl (–OH) functionality or anionic carboxyl group. Cationic surfactants are not used in wafer cleaning since they tend to adsorb on almost all polymeric surfaces such as cassettes. Surfactants that cause significant foaming can leave stains on the wafer surface if not removed properly after wafer cleaning [60]. To reduce or eliminate foaming, defoamers may
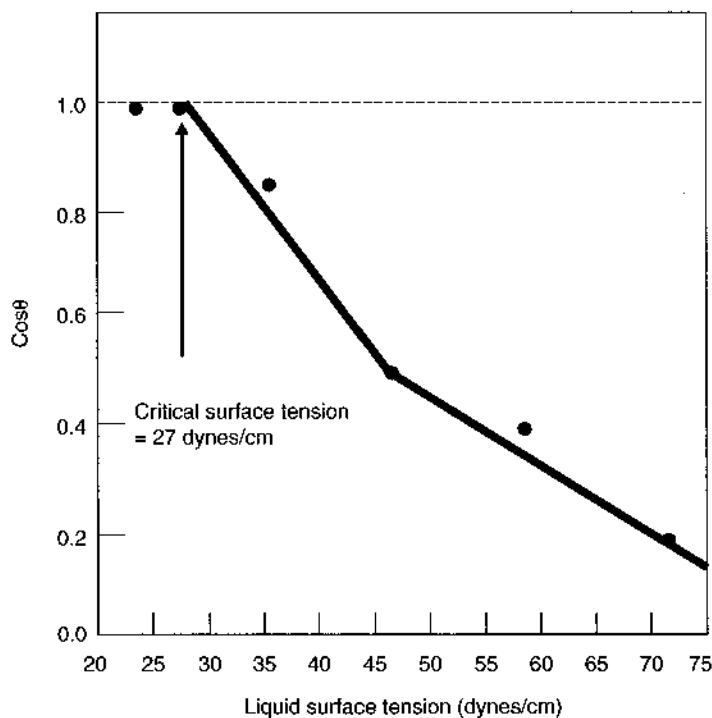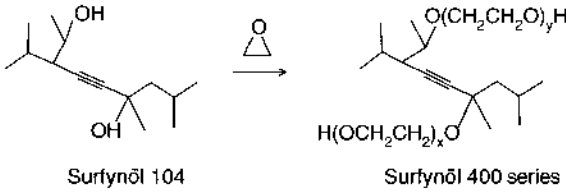
Figure 1.14. Zisman plot for methanol-water solutions on a silicon substrate. Plot gives $\gamma_c = 27$ dyne/cm [59]. Redrawn with permission of ECS – The Electrochemical Society from Gould, G. and Irene, E. A., *Journal of the Electrochemical Society*.

be added. Hydrofluoric acid-based etching or cleaning solutions may contain anionic or non-ionic surfactants for improving wettability of silicon [61] and a hydrophobic base to enhance penetration of trenches. Block copolymers containing polyethylene oxide (PEO) and polypropylene oxide (PPO) groups can also be used as surfactants. Chapter 4 discusses the uses of surfactants in cleaning solutions. Some generic structures of surfactants of interest to wafer cleaning are listed in Table 1.3.

Surfactants have a tendency to adsorb at solution/air and solid/liquid interfaces resulting in the reduction of interfacial tension [62] [63]. In Figure 1.15, the surface tension of 1 wt% HF solution is shown as a function of the concentration of a polyglycidol based nonionic surfactant (Arch Chemicals Inc.OHS®) [64]. The graph shows that by adding a surfactant the surface tension of HF can be significantly reduced even at very low (tens of ppm) concentrations. The critical micelle concentration (CMC) may be estimated to be roughly 90 ppm. Increasing the ionic strength of a cleaning solution will decrease the CMC of the surfactant [65]. The CMC value of a given surfactant would be lower in BHF solutions that have much higher ionic strengths than an HF solution without another component.

Surfactant adsorption at a solid/liquid interface can modify the wettability of the surface. Dynamic contact angle measurements carried out using a Wilhelmy plate technique on hydrogen-terminated silicon show a broad hysteresis loop in deionized water – the advancing and receding angles are 87° and 61°, respectively, as shown in Figure 1.16a [64]. The contact angles in 100:1 HF solution have

Table 1.3. Generic structures of some surfactants of interest to wafer cleaning.

Surfactant	Generic Structure
Non ionic	
Alkyl phenoxy polyglycidol (OHS®)	R-Ph-O-$(CH_2CH(OH)CH_2O)_n$-H
Acetylenic alcohols (Surfynol)	 Surfynōl 104 → Surfynōl 400 series S420, x + y = 1.2 S440, x + y = 3.5 S465, x + y = 10 S485, x + y = 30
Alkyl phenoxy polyethylene alcohols (NCW)	RO$(CH_2CH_2O)_l(CH(CH_3)CH_2O)_m(CH_2CH_2O)_n$H R = $C_{12}H_{25}/C_{14}H_{29}$, l + n = 10, m = 4.5
Anionic	
Low chain carboxylates	R-COO- M+, where R = hydrocarbon or a fluorocarbon
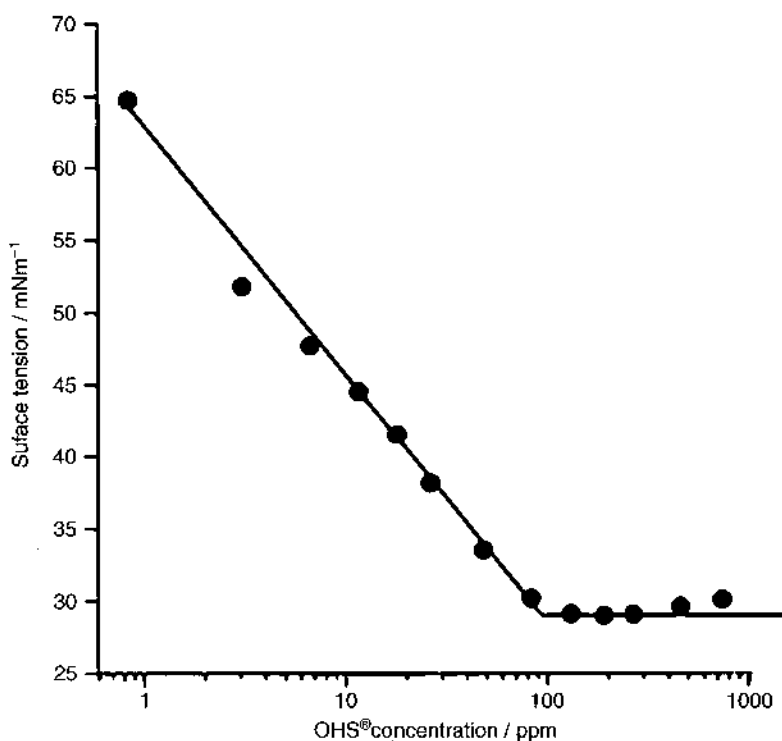
Figure 1.15. Surface tension *vs.* concentration of a nonionic surfactant in 1 wt% HF solution [64]. Reproduced with permission of ECS – The Electrochemical Society from Haworth, P., Kovach, M., Sperline, R., and Raghavan, S., *Journal of the Electrochemical Society*.

Figure 1.16. Advancing and receding contact angles of a) DIW on hydrogen terminated silicon, and b) 100:1 HF on silicon as a function of OHS® concentration (●) cycle 1 advancing, (■) cycle 2 advancing, (▲) cycle 1 receding, (▼) cycle 2 receding [64]. a) Used with permission from authors. b) Reproduced with permission of ECS – The Electrochemical Society from Haworth, P., Kovach, M., Sperline, R., and Raghavan, S., *Journal of the Electrochemical Society.*

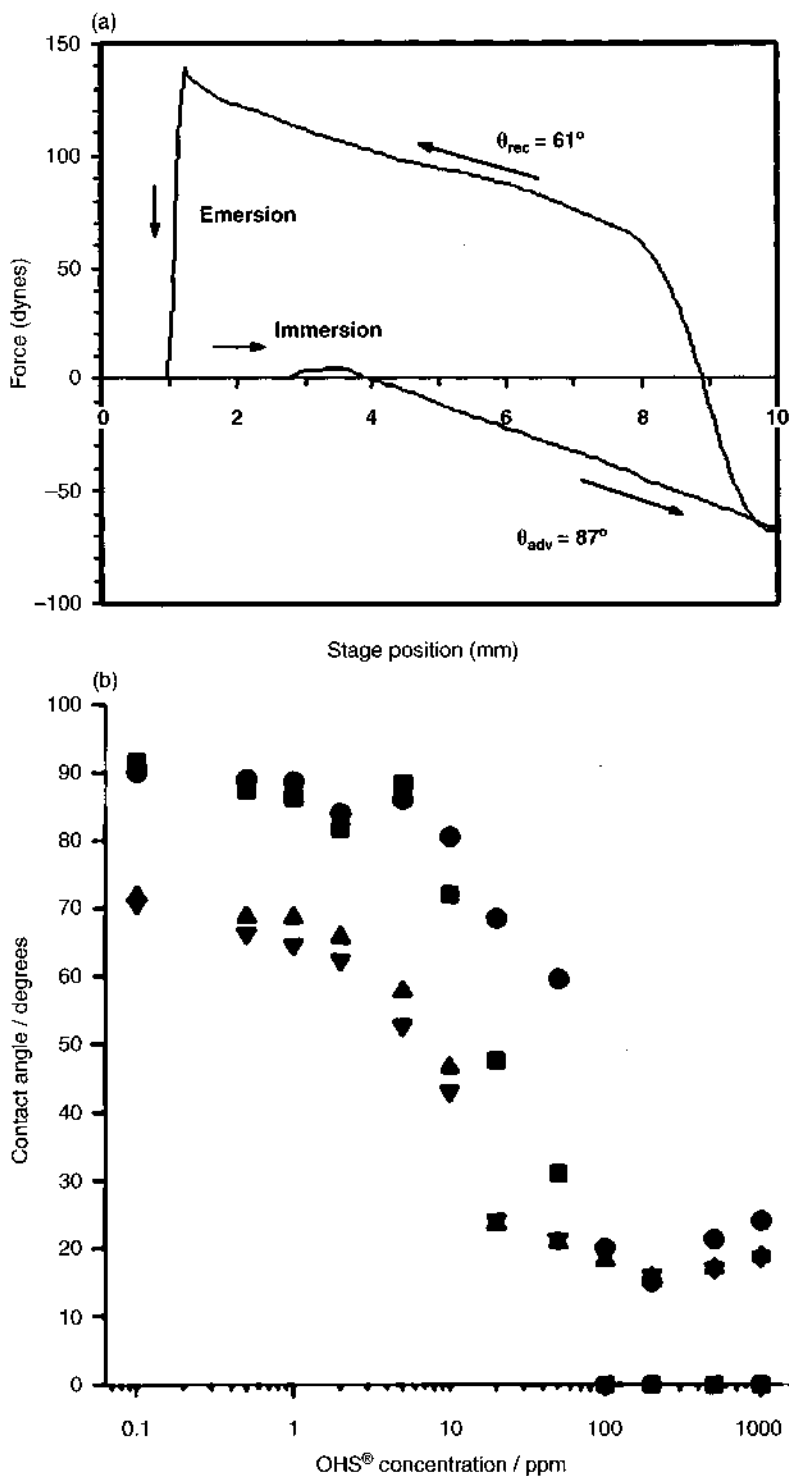been measured to be approximately the same. When 10 ppm of OHS® surfactant is added to a 100:1 HF solution, the advancing and receding angles decrease to 74° and 44°, respectively, clearly confirming enhanced wettability (as shown in Figure 1.16b). At a value close to the CMC of the surfactant, the surface becomes highly wettable with solution contact angles less than 20°. Interestingly, when two immersion cycles are used, the advancing contact angle becomes zero during the second cycle (the square data points in Figure 1.16b).

The adsorption/desorption characteristics of surfactants on silicon has been investigated [66, 67] using attenuated total reflection-Fourier transform infrared spectroscopy (ATR-FTIR) [68, 69]. Interaction of hydrocarbon surfactants such as poly(ethylene oxide alcohol) and polyglycidol-type surfactant (OHS®) with hydrofluoric acid can be followed by monitoring the intensity of –C-H peaks in the 2800–3000 cm^{-1} range. In BHF solutions, absorption due to –N-H groups from NH_4^+ ions in solution strongly interferes with the –C-H peaks in adsorbed surfactant species. The N-H stretching is lowered from 3200 cm^{-1} to 2850 cm^{-1} due to hydrogen bonding [70, 71]. A technique based on replacement of the ammonium ions close to the silicon surface by alkali cations has been demonstrated to overcome the interference due to the large number of NH_4^+ ions in solution [67]. A comparison of adsorption density of OHS® onto silicon from 7:1 BHF solution (7 parts of NH_4F [40 wt%] and 1 part of HF [49 wt%]) with that from 50:1 HF solutions for various OHS® concentrations is shown in Table 1.4. The adsorption from BHF solution is approximately 20% higher than that from dilute HF solutions.

1.6   High Aspect Ratio Cleaning: Narrow Structures

Wet chemical cleaning of narrow vias and trenches requires efficient, complete, and fast penetration of cleaning chemicals. Thus, both thermodynamic and kinetic factors are important. Liquid penetration by capillary effect primarily

Table 1.4. Comparison of OHS® equilibrium adsorption densities onto silicon from 50:1 HF solutions and 7:1 BHF solutions [67]. Reprinted with permission from Almanza-Workman, A., Raghavan, S., and Sperline, R., *Langmuir*, 16(6):3636. Copyright 2000 American Chemical Society.

Surfactant (OHS®) concentration (ppm)	Equilibrium adsorption onto silicon Γ_{OHS}® (mol/cm²)	
	50:1 HF (I ~ 1.4 M)	7:1 BHF (I ~ 12 M)
5	$9.13 \times 10^{-11} \pm 0.5 \times 10^{-11}$	1.15×10^{-10} (using KF/HF, I ~ 8 M) 1.17×10^{-10} (using CsF/HF, I ~ 12 M)
100	$1.59 \times 10^{-10} \pm 0.1 \times 10^{-10}$	1.93×10^{-10} (using KF/HF, I ~ 8 M) 1.91×10^{-10} (using CsF/HF, I ~ 12 M)
500	$2.93 \times 10^{-10} \pm 0.2 \times 10^{-10}$	3.66×10^{-10} (using KF/HF, I ~ 8 M) 3.58×10^{-10} (using CsF/HF, I ~ 12 M)

I = calculated ionic strength in solution

depends upon the contact angle of the liquid on the walls of the vias/trenches, which should be as small as possible. It is also important for the liquid surface tension to be roughly the same as the critical surface tension of wetting of the via/trench material. The rate of penetration is controlled by contact angle, feature dimensions, and viscosity of the liquid. Narrower and deeper trenches can be expected to have lower rates of liquid penetration making cleaning of high aspect ratio features difficult.

1.6.1   Rate of Liquid Penetration into Narrow Structures

The rate of advance of liquid into an air-filled via, theoretically of any width, can be calculated using Rideal-Washburn equation [72, 73]:

$$\frac{dl}{dt} = \frac{r\gamma cos\theta}{4\eta l} \tag{1.18}$$

where r, γ, h, l, θ refer to the radius of the via, the surface tension of the liquid, the viscosity of the liquid, length of the via and contact angle of the liquid on the solid, respectively. This equation can be easily derived from Poiseuille's equation of flow through a capillary tube assuming that the driving pressure is due to positive Laplace pressure ($= 2\,\gamma\,cos\theta/\,r$), and the liquid-vapor meniscus is hemispherical. Equation 1.18 can be integrated and rearranged to calculate time for complete penetration into the via as follows:

$$t = \frac{2\eta l^2}{r\gamma cos\theta} \tag{1.19}$$

As evident from the above equation, smaller values of $\gamma\,cos\theta$ increase the time required for filling of hydrophilic vias (for hydrophobic [$\theta > 90°$] vias, Laplace pressure is negative) .

Olim derived an expression for filling of hydrophilic trenches (of width w) closed at one end [74]. His derivation is based on the fact that hydrophilic walls of the feature create a concave surface at the gas/liquid interface and the resulting Laplace pressure increases the pressure in the gas trapped in the feature. The pressurized gas dissolves into the liquid, thus, allowing the liquid to fill the feature.

To estimate the upper bound of the time required to fill the feature, Olim made the following assumptions:

1. The gas/liquid interface is saturated.
2. The process is isothermal.
3. There is no change in curvature of liquid/vapor interface.
4. The rate of gas diffusion from the interface into the liquid is proportional to the concentration gradient at the interface, dC/dn where C is the molar concentration of the dissolved gas and n is distance normal to the interface.
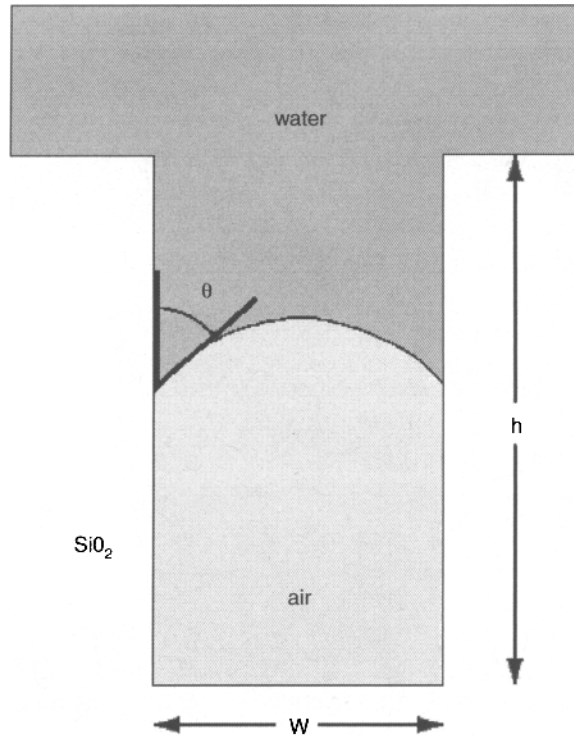
Figure 1.17. Schematic showing feature wetting of a high aspect ratio via or contact [74]. Where w is the width, h is the height and θ is the contact angle. This shows a low surface energy solution with a convex angle indicating a hydrophilic surface. Reproduced with permission of ECS – The Electrochemical Society from Olim, M., *Journal of the Electrochemical Society.*

The conditions at which this gradient is minimized yields the slowest diffusion rate and that in turn yields an upper limit on the value of the time interval required for the liquid to fill the feature, $\Delta t_{fill,max}$, which is given by [74]:

$$\Delta t_{fill,max} = \frac{k}{DRT}\left[1 + \frac{P_h}{\Delta P}\right]h^2 \tag{1.20}$$

where k, D, R, T, P_h, ΔP, and h are Henry's constant, diffusion coefficient of the gas in the liquid, universal gas constant, gas temperature, atmospheric pressure, pressure difference across the liquid gas interface, and feature depth, respectively.

Replacing ΔP by $2\gamma cos\theta/w$, Eq. 1.20 becomes:

$$\llbracket\Delta t\rrbracket_{(fill,max)} = k/DRT[1 + (P_{hw})/2(cos\theta)h^2 \tag{1.21}$$

It may be noticed from Eq. 1.21 that maximum filling time is a function of feature dimensions h and w, surface tension of the liquid filling the feature γ, contact angle at the liquid-vapor interface θ, Henry's constant k, diffusion coefficient, D, of gas in

liquid and temperature of liquid. The equation predicts a filling time of ~1 sec for water at 300 K in trenches 0.5 μm wide and 4 μm deep. The filling time increases for narrower and deeper trenches and can go up to ~10 sec for features 1 μm wide and 10 μm deep.

Ota *et al.* predicted the liquid infiltration rate into wettable and non-wettable 2-μm deep trenches/microholes in the size range of 0.2 to 1.6 μm [75]. The model for infiltration rate was based on the overall force balance due to liquid pressure, gas pressure inside the trench prior and during the fill process, and the Laplace pressure. The overall force (F) balance during initial infiltration stage for non-wetting and wetting liquids is given by Eq. 1.22 and 1.23, respectively. In these equations, the first two terms on the right refer to liquid pressure, the second term to gas pressure inside the microhole, and the third term to pressure due to surface tension:

$$F = \left\{ P_0\pi\left(\frac{d}{2}\right)^2 + s\rho g\left(\frac{d}{2}\right)^2 \right\} - P_i\pi\left(\frac{d}{2}\right)^2 - T\sin\alpha\, 2\pi\left(\frac{d}{2}\right) \tag{1.22}$$

$$F = \left\{ P_0\pi\left(\frac{d}{2}\right)^2 + s\rho g\left(\frac{d}{2}\right)^2 \right\} - P_i\pi\left(\frac{d}{2}\right)^2 + T\cos\beta\, 2\pi\left(\frac{d}{2}\right) \tag{1.23}$$

In the above equations, d is the microhole diameter, P_0 is the outside liquid pressure, P_i is the inside gas pressure, s is the liquid thickness above the microhole, ρ is the liquid density, g is the acceleration due to gravity, T is the liquid surface tension, and α and β are the contact angles of liquid on non-wettable and wettable microholes respectively.

Since, $P_0 = P_i$ initially, and assuming pressure due to liquid head ($s\rho g$) to be negligible, Eq. 1.22 and Eq. 1.23 convert to

$$F = -T\sin\alpha\, 2\pi\left(\frac{d}{2}\right) < 0 \tag{1.24}$$

$$F = +T\cos\beta\, 2\pi\left(\frac{d}{2}\right) > 0 \tag{1.25}$$

The net negative force for non-wettable surface suggests that liquid does not infiltrate into microhole of such a surface. On the other hand, net positive force for wettable surface indicates that liquid is able to penetrate into a microhole irrespective of its size.

As the liquid starts penetrating into the wettable micropore, the pressure inside the gas phase in the micropore increases and at equilibrium, the liquid penetrates to a depth h. The force balance in this case is:

$$F = \left\{ P_0\pi\left(\frac{d}{2}\right)^2 + h\rho g\left(\frac{d}{2}\right)^2 \right\} | P_i\pi\left(\frac{d}{2}\right)^2 + T\cos\beta\, 2\pi\left(\frac{d}{2}\right) = 0 \tag{1.26}$$

Considering $h\rho g$ being negligible compared to other terms in the equation, Eq. 1.27 is obtained. Additionally, a force balance between pressure inside the gas phase in

the microhole and the water pressure yields Eq. 1.28, where L is the total depth of the microhole and P_{ini} is the initial pressure in the gas phase of the microhole:

$$\left\{ (P_0 - P_i) + \frac{4T}{d} \cos \beta \right\} = 0 \tag{1.27}$$

$$P_i(L - h) = P_{0u}L \tag{1.28}$$

Combining Eq. 1.27 and Eq. 1.28, and assuming that no dissolution of gas occurs (different from Olim's approach [74]) in the liquid inside the microhole, Eq. 1.29 is obtained:

$$\frac{h}{L} = 1 - \frac{1}{\dfrac{P_o}{P_{oa}} + \dfrac{4T\cos\beta}{P_{02}d}} \tag{1.29}$$

This equation shows that the extent of liquid infiltration (which Ota and Tsutsumi describe as infiltration rate), h/L, depends on initial pressure in the gas phase of the microhole, liquid pressure, surface tension of the liquid, micropore size, and contact angle of liquid on the microhole surface. Conditions that will promote good penetration (h/L approaching 1) include low values of P_{on}, d, and β, and high values of T. The authors of [75] have shown experimentally that the extent of liquid infiltration is about 0.75 for wettable microholes (contact angle = 28°) in the size range of 0.2 to 1.0 µm. The experimentally determined infiltration values matched well to those predicted with the theoretical model.

1.6.2   Enhancement of Liquid Penetration into Narrow Structures

Efficient cleaning of surfaces and deep vias/trenches is critical to the semiconductor industry. Considerable work has been done to understand particle/ionic contaminant removal mechanisms in megasonic cleaning of both blanket and patterned wafers [76, 77]. It has been shown that oscillating flow (vortex oscillating mechanism) generated in a megasonic process provides a significant advantage in terms of reducing the rinsing time for patterned wafer cleaning [77].

1.7   Surface Tension Gradient: Application to Drying

Drying is an integral part of cleaning. Improper drying can leave watermarks on a wafer surface that can act as undesirable masks during subsequent processing, such as etching and deposition [78, 79]. Additional challenges exist in drying surfaces that consist of hydrophilic and hydrophobic regions in close proximity. Spin drying does not reduce the thickness of the water layer on a hydrophilic wafer below 0.5 µm in the typical wet processing time. Using evaporation to remove this water layer is known to leave watermarks on the surface. To reduce or prevent the formation of these watermarks, drying based on a surface tension gradient by use of isopropyl alcohol is commonly carried out as discussed in the following section.

1.7.1   Isopropyl Alcohol Surface Tension Gradient Drying

One of the most important steps in wet processing of wafers is drying. While the use of isopropyl alcohol (IPA) in removing water from wafer surfaces has been practiced for over three decades, the manner in which isopropyl alcohol is used has changed significantly [80]. Drying methods based on IPA to remove water from wet wafers include condensation of hot IPA on a wafer to "dissolve away" water [81], direct displacement of water by liquid IPA [82], and creation of a surface tension gradient using dilute IPA vapor at ambient temperature [83–85]. Drying by condensation of hot IPA vapor in almost pure form or of an azeotropic composition by condensing on the wafer – vapor drying, has been replaced by drying using IPA vapors, typically in an N_2 atmosphere, at ambient temperatures, condensing the IPA on the water surface, in which the wafers are submerged, and then slowly raising the wafers (or lowing the water). This latter drying method, known as surface tension gradient (STG) drying or Marangoni drying, is based on the ability of IPA to reduce the surface tension of water along with the creation of gradient of surface tension on a water meniscus formed on a wafer surface.

The creation of a surface tension gradient on a water meniscus (*i.e.* water/vapor interface) formed on a hydrophilic wafer is shown in Figure 1.18. Exposure of this meniscus to IPA vapor (typically diluted with nitrogen to 1–2 vol%) results in the adsorption of IPA molecules at the water/vapor interface. Since IPA is soluble in water, the adsorbed IPA molecules tend to diffuse into the bulk water. As shown in Figure 1.18, at a location far away from the wafer surface (*C*), diffusion of adsorbed IPA molecules into the water would result in a low density of molecules on the surface. In a region very close to the wafer surface (*A*), diffusion of IPA molecules is reduced due to the very thin water layer; consequently, the surface concentration of molecules is larger than that in region *C*. In the region *B*, the surface concentration of IPA molecules would be between that in region *A* and region *C*. Variation in the surface concentration of IPA molecules would result in a gradient of increasing surface tension from region *A* to *C*. In an attempt to reach equilibrium, the IPA molecules flow from region *A* towards region *C* and carry water molecules with them. This movement creates motion of a few subsurface layers dictated by the fact that the surface tension force is balanced by viscous forces. Once the water is stripped away by the surface tension effect, the IPA easily evaporates, and the wafer is rendered dry.

The surface tension of water/IPA solutions is plotted in Figure 1.19 as a function of volume percent of IPA in solution [83]. Addition of IPA in water up to 20 vol% decreases the surface tension of water steadily from 72 mN/m to roughly 32 mN/m. This is due to the population of IPA molecules at the solution/air interface. Beyond 25 vol% IPA, the change in surface tension is minimal due to progressive saturation of the interface with IPA molecules.

1.7.2   Water Layer After Drying

"Stripping" of layers of water by the surface tension gradient effect dries the wafer. In order to maintain the STG effect, there has to be relative motion between the wafer and the water in the rinse bath. A fluid mechanics based model relevant to
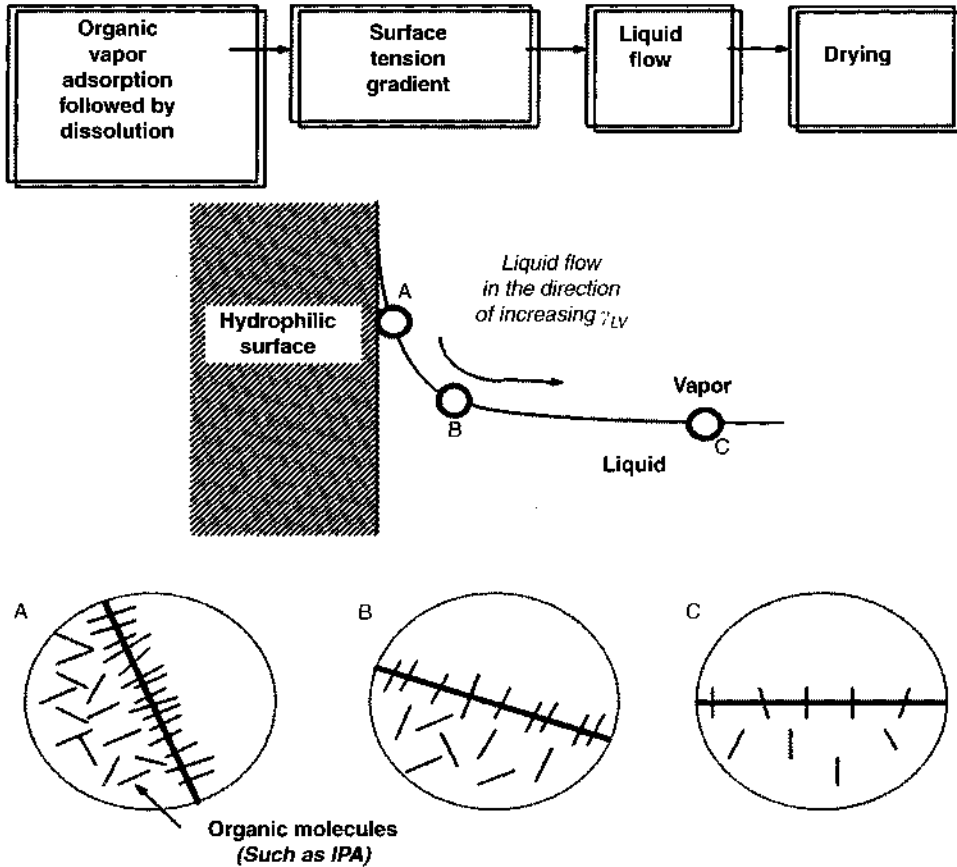
Figure 1.18. Schematic figure showing the surface tension gradient at the liquid-vapor interface on a hydrophilic surface. The difference in surface concentrations of IPA molecules at three locations *A, B, and C* is also illustrated. Used with permission from the authors.

Marangoni drying has been developed by Thess and Boos [85]. This model which assumes that the surface tension distribution is a known function of position and attempts to explain the movement of a thin liquid film on a flat plate that is vertically withdrawn from a large liquid reservoir in the presence of a surface tension gradient.

The beneficial effects of IPA in reducing the thickness of the evaporated water layer have been elegantly shown by researchers at FSI. Figure 1.20 clearly shows that low liquid drain rates (rate of movement of liquid/vapor interface along the wafer) of 1 to 2 mm/sec along with IPA vapor can tremendously reduce the thickness of the water layer.

1.7.3 Alternate Chemicals for Drying

In principle, any organic vapor that is capable of adsorbing at the water/vapor interface as well as dissolving in water could be used for STG drying. However, the work of Marra *et al* [83] showed that the efficacy of organic vapors meeting
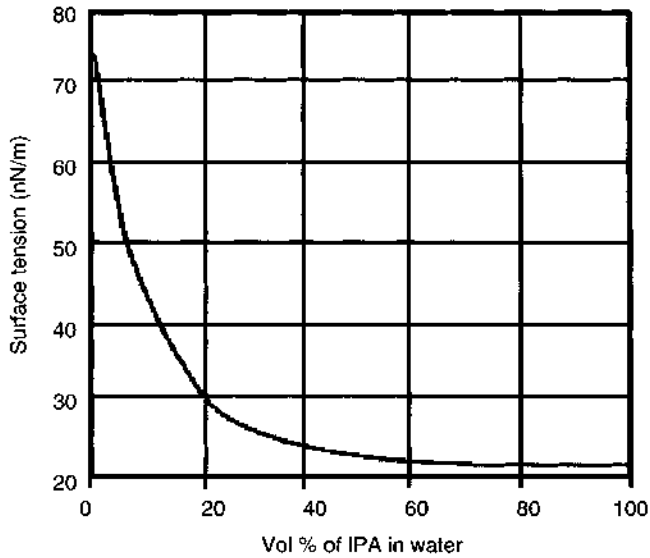
Figure 1.19. Surface tension of water (mN/m) as a function of volume percent of IPA in water [87]. Used with permission from Jin-Goo Park.
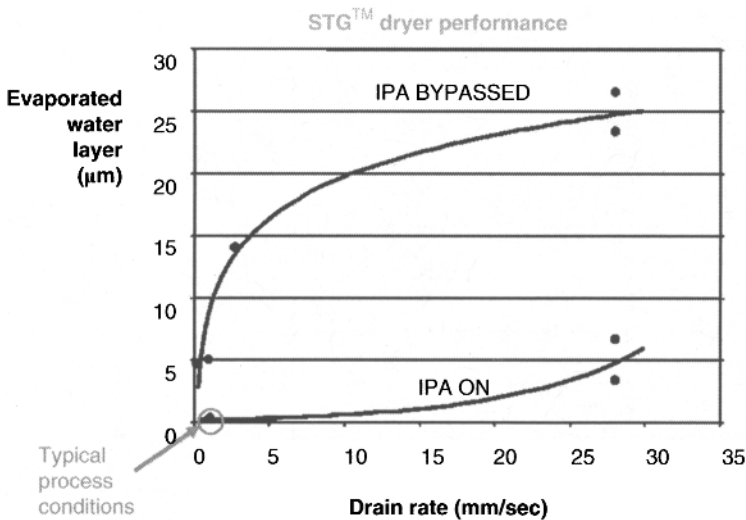
Figure 1.20. Effect of liquid drain rates along with IPA vapor on thickness of water layer. Courtesy of FSI International, Inc.

both of these criteria in providing drying varies widely. For example, they found acetone to be less effective than IPA. Leenaars *et al.* compared the drying performance of several organic vapors and emphasized the importance of optimum vapor pressure and water solubility of vapors in drying of wafers [88]. Table 1.5 provides selected physical constants and drying results for organic solvent investigated by these authors [88, 89]. To date, the reason for the superior

Table 1.5. Marangoni drying result and selected physical constants for various organic vapors. Table adapted from [88, 89].

Solvent	Drying Result	Saturation Vapor Pressure (mbar)	Solubility (g/L of water)	Surface Tension of Solvent mNm^{-1}
2-Proponal	+	43	Complete	20.93
1-Proponal	+	19	Complete	23.32
2-Butanol	+/−	17	125	22.54
1-Hexanol	+/−	1	5.8	25.81
1-Heptanol	−	0.5–1	<1	38.50
1-Octanol	−	0.3	0.54	27.10
Hexane	−	160	0.05	17.89
Tetrachloro-Methane	−	120	0.8	26.43
Octane	−	15	0.1	21.14
Diethyl Ether	−	587	12	16.65
Ethyl Acetate	++	97	80	23.39
Butyl Acetate	++	13	10	24.88
Methyl Isobutyl Ketone	++	6.7	19	25.45
Acetone	+	233	Complete	22.72
Tetrahydrofuran	++	200	Complete	23.97
2-Ethoxy Ethanol	++	5	Complete	28.35
Diacetone Alcohol	++	1.5	Complete	24.88
1-Methyl -2-Pyrrolidone	+	0.3	Complete	28.91
Ethylene Glycol	−	0.06	Complete	47.99
Nitrogen	−	1000	0.02	−

Vapor flow of 6 L/min, drying result: '−' = bad, '+/−' = moderate, '+' = good, '++' = excellent, solubility/vapor pressure at 20°C, surface tension at 25°C

performance of IPA in providing drying by STG effect has not been clearly established. Because of flammability issues related to IPA (flash point of IPA is ~12°C), there has been interest in replacing IPA with nonflammable liquids such as methoxy–nonafluorobutane based fluids, manufactured by 3M under the trade name Novec™.

1.8   Summary

In this chapter, we have reviewed some of the fundamentals of surface chemical concepts involved in wet chemical cleaning and drying of surfaces pertinent to integrated circuit fabrication. Improvement in cleaning and drying of surfaces is possible through a basic understanding of interfacial phenomena. It is pertinent to mention that much of the fundamental principles described in this chapter were known as early as the 1950's. However, due credit must be given to the semi-conductor industry for taking these principles further and implementing them in wafer cleaning and drying applications.

References

1. Yopps, J. A., and Fuerstenau, D. W., *J. Colloid Sci.*, 19(1), 61 (1964).
2. Mueller, R., Langmuir, 19(1), 160–165, (2003).
3. Stumm, W., *Aquatic Chemistry: Chemical Processes at the Particle-water Interface*, p. 83, John Wiley & Sons, Inc., New York (1987).
4. Knotter, D. M., *J. Am. Chem. Soc.*, 122(18):4345 (2000).
5. Fuerstenau, D. W. and Healy, T. W., *Principles of Mineral Flotation*, pp.100–101, Academic Press, Inc., New York and London (1972).
6. Busnaina, A., Park, J., and Bakhtari, K., Chapter 3, *Handbook of Silicon Wafer Cleaning Technology*, Second Edition, (Reinhardt, K. A. and Kern, W., eds.) William Andrew Publishing, New York, (2007).
7. Kotz, J. C, Treichel. P, and Townsend, J. R, *Chemistry and Chemical Reactivity*, 7th Edition Volume 1, p. 790, Brooks/Cole Publishing Co. (2008).
8. Gaudin, A. M. and Fuerstenau, D. W., AIME (Mining Engineering) Trans., 202:66 (1955).
9. Iwasaki, I., Cooke, S. R. B., and Choi, H. S, AIME (Mining Engineering) Trans., 220:394 (1961).
10. Berube, Y. G. and deBruyn, P. L., *J. Colloid Interface Sci.*, 27(2):305 (1968).
11. Parks, G. A., *Chem. Rev.*, 65(2):177 (1965).
12. Parks, G. A., *Advan. Chem. Ser.*, 67(6):121 (1967).
13. Ohsawa, K., Murata, O. M and Ohshima, H., *Colloid and Polymer Sci.*, 264(12):1005 (1986).
14. Noh, J. S and Schwarz, J. A., *J. Colloid Interface Sci.*, 130(1):157 (1989).
15. Noh, J. S. and Schwarz J. A., *Carbon*, 28(5):675 (1990).
16. Zalac, S., and Kallay, N., *J. Colloid Interface Sci.* 149(1):223 (1992).
17. Xie, F., Phillips, J., Silva, I., F., Palma, M. C., and Angel Menéndez, J., *Carbon*, 38(5):691 (2000).
18. Valdés, H., Sánchez-Polo, M., Rivera-Utrilla, J., and Zaror, C., A., *Langmuir*, 18(6):2111 (2002).
19. Stumm, W., *Chemistry of the Solid-Water Interface*, pp. 87–155, John Wiley & Sons Inc., New York (1992).
20. Knotter, D. M., Stewart, N., and Sharp, I., *Solid State Phenomena*, 103–104:103 (2005).
21. Binnig, G., Quate, C. F., and Gerber, C., *Phys. Rev. Lett.*, 56(9):930 (1986).
22. Jan, D. and Raghavan, S., *J. Electrochem. Soc.*, 141(9):2465 (1994).
23. Von Helmholtz, H. L. F, *Ann. Phys. Chem.*, (Ser. 1) 89:211 (1853).
24. Gouy, G. J., *J. Phys.*, 9:457 (1910).
25. Chapman, D. L., *Phil. Mag.*, 25:475 (1913).
26. Stern, O., *Z. Electrochem.* 30:508 (1924).
27. Lyklema, J., *Fundamentals of Interface and Colloid Science*, Volume 2, p. 3.208, Academic Press, London (1995).
28. Kruyt, H. R., *Colloid Science*, Volume 1, Elsevier Publishing Co., Amsterdam (1952).
29. Hunter, R.J., *Zeta Potential in Colloid Science: Principles and Applications*, Academic Press, London (1988).
30. Hunter, R. J., *Introduction to Modern Colloid Science*, Oxford University Press, Oxford, United Kingdom (1994).

31. Fuerstenau, D. W., *The Adsorption of Surfactants at Solid-Water Interfaces, The Chemistry of Biosurfaces*, Volume 1, p. 143, (Hair, M. L., ed.), Marcel Dekker Inc., New York (1971).
32. Black, A. P. and Smith, A. L., *J. Am. Water Works Assoc.*, 54: 926 (1962).
33. Chilkunda, R., *Fundamental aspects of particulate contamination of tungsten and thermal oxide wafers during chemical-mechanical polishing*, Ph.D. Dissertation, The University of Arizona, p.111 (1997).
34. Bu, K. and Moudgil, B., *Chemical-Mechanical Planarization – Integration, Technology and Reliability, Mater. Res. Soc. Symp. Proc.*, 867:W8.5.1 (Kumar, A., Lee, J. A., Obeng, Y. S., Vos, I., and Johns, E. C., eds.) (2005).
35. Lowalekar, V., Raghavan, S., Pandit, V., Parks, H., and Jeon, J., *J. Appl. Phys.*, 99(2):4503 (2006).
36. Bellmann, C., Opfermann, C., Jacobasch, A., and Adler, H.-J., *Fresenius J. Anal. Chem.*, 358(10):255 (1997).
37. Hiemenz, P. C. and Rajagopalan, R., *Principles of Colloid and Surface Chemistry*, Third Edition, p. 546 Marcel Dekker, Inc., New York (1997).
38. Bergstrom, L. and Pugh, R. J., *J. Am. Ceram. Soc.*, 72(1):103 (1989).
39. Oliveira, M., Chen, K., and Ferreira, J., *J. Eur. Ceram. Soc.*, 21(13):2413 (2001).
40. Derjaguin, B. V. and Landau, L. D., *Journal of Experimental and Theoretical Physics*, 11(12):802 (1941).
41. Derjaguin, B. V.and Landau, L. D., *Acta Phys.-Chim. URSS*, 14(6):633 (1941).
42. Verwey, E. J. W., Overbeek, J. Th. G., *Theory of the Stability of Lyophobic Colloids*, p. 108, Elsevier Publishing Co., Amsterdam (1948).
43. Riley, D. J and Carbonell, R. G., *J. Colloid Interface Sci.*, 158(2):259 (1993).
44. Rosato, J, Hall, R., Parry, B, Lindquist, G, and Jarvis, D, *Ultraclean Semiconductor Processing Technology and Surface Chemical Cleaning and Passivation, Mat. Res. Soc. Symp. Proc.*, 386:O-127 (Liehr, M., Heyns, M., Hirose, M., and Parks, H., eds.) (1995).
45. Chen, Z. and Singh, R. K., *J. Electrochem. Soc.*, 150(11):G667 (2003).
46. Ducker, W. A., Senden, T. J., and Pashley, R. M., *Nature*, 353:239 (1991).
47. Ducker, W. A., Senden, T. J., and Pashley, R. M., *Langmuir*, 8(7):1831 (1992).
48. Cooper, K., Gupta A., and Beaudoin, S., *J. Colloid Interface Sci.*, 228(2):213 (2000).
49. Loewenstein, L., Charpin, F., and Mertens, P., *Journal of The Electrochemical Society*, 146, 2, pp. 719–727 (1999)
50. Yiacoumi, S. and Tien, C., *J. Colloid Interface Sci*, 175(2):333 (1995).
51. Ritchie, G. S. P., and Jarvis, S. C., *J. Soil Sci.*, 37(2):205 (1986).
52. Deng, S., Bai, R., and Chen, J. P., *J. Colloid Interface Sci.*, 260(2):265 (2003).
53. Huang, H. H., STABCAL, University of Montana (1995).
54. Vazquez-Arenas, J., Lazaro, I., and Cruz, R., *Electrochimica Acta*, 52(20):6106 (2007).
55. Lee, W., Torek, K. J., Palsulich, D. A., and Weston, L., *Science and Technology of Semiconductor Surface Preparation, Mat. Res. Soc. Symp. Proc.*, 477:57 (Higashi, G., Hirose, M., Raghavan, S., and Verhaverbeke, S., eds.) (1997).
56. James, R. O. and Healy, T. W., *J. Colloid Interface Sci.*, 40(1):42 (1972).
57. James, R. O. and Healy, T. W., *J. Colloid Interface Sci.*, 40(1):53 (1972).
58. Zisman, W. A., *Contact Angle, Wettability, and Adhesion*, Chapter 1 (Gould, R. F., ed.) American Chemical Society, Washington D.C., (1964).
59. Gould, G. and Irene, E. A., *J. Electrochem. Soc.*, 135(6):1535 (1988).
60. Beyer, M., Budde, K., and Holzapfel, W., *Appl. Surf. Sci.*, 63(1–4):88 (1993).
61. Kikyuama, H., Miki, N., Saka, K., Takano, J., Kawanabe, I., Miyashita, M., and Ohmi, T., *IEEE Trans. Semiconduct. Manufact.*, 4(1):26 (1991).
62. Rosen, M., *Surfactants and Interfacial Phenomena*, 3rd Edition, pp. 208, John Wiley & Sons, Inc., New York (2004).
63. Myers, D., *Surfactant Science and Technology*, 3rd Edition, John Wiley & Sons, Inc., New York. (2006).
64. Haworth, P., Kovach, M., Sperline, R., and Raghavan, S., *J. Electrochem. Soc.*, 146(6):2284 (1999).
65. Emerson, M. F. and Holtzer, A., *J. Phys. Chem.*, 71(6):1898 (1967).
66. Jeon, J., *Applications of ATR FT-IR and wettability techniques in the study of solid/liquid interfacial phenomena*, Ph.D. dissertation, The University of Arizona, (1993).
67. Almanza-Workman, A., Raghavan, S., and Sperline, R., *Langmuir*, 16(6):3636 (2000).
68. Griffiths, P., and De Haseth, J. A., *Fourier Transform Infrared Spectrometry*, 2nd Edition, p. 321, John Wiley & Sons Inc., New York (2007).

69. Smith. B. C., *Fundamentals of Fourier Transform Infrared Spectroscopy*, 2nd Edition, CRC Press, New York (2010).

70. van de Voort, F.R., Mills, B. L., Paquette, G. A., and Grunfeld, E., *J. Assoc. Off. Anal. Chem.*, 69(6):924–8 (1986).

71. Czugler, M., Kótai, L., Sreedhar, B., Rockenbauer, A., Gács, I., and Holly, S., *Euro. J. Inorg. Chem.*, 2002(12):3298 (2002).

72. Washburn, E. D., *Phys. Rev.*, 17(3):273 (1921).

73. Rideal, E. K., *Phil. Mag.*, 44(264):1152 (1922).

74. Olim, M., *J. Electrochem. Soc.*, 144(12):4331 (1997).

75. Ota, K., and Tsutsumi, A., ECS Transactions, 11(2), pp. 299–306 (2007)

76. Keswani, M., Raghavan, S., Deymier., and Verhaverbeke, S., *Microelectronic Engineering*, 86(2):132 (2009).

77. Lin, H., Busnaina, A., and Suni, I., *IEEE Interconnect Technology Conference Proceedings*, p. 49 (2000).

78. Matsuzaki, H., Ookouchi, I., Kurokawa, H., Ebara, K., and Takahashi, S., *J. Chem. Engr. Jpn.*, 21(5):490 (1988).

79. Park, J. G. and Pas, M. F., *J. Electrochem. Soc.*, 142(6):2028 (1995).

80. Funkhänel, J. and Schupke, K., *Semiconductor International*, 27(11):55 (2004).

81. Chang, I., and Kim, J., *Journal of Cleaner Production*, 9(3): 227 (2001).

82. Zant, P., Microchip Fabrication, 5th Edition, McGraw-Hill, p. 134 (2004)

83. Marra, J., and Huethorst, J. A. M., *Langmuir*, 7(11):2748 (1991).

84. Wolke, K., Eitel, B., Schenkl, M., Ruemmelin, S., and Schild, R., *Solid State Technology*, 39 (8):87 (1996).

85. Thess. A., and Boos, W., *Phys. Fluids*, 11(12):3852 (1999).

86. Park, J. and Raghavan, S., *Microcontamination*, 10(10):54-3 (October, 1992).

87. Park, J., *Wettability aspects during silicon wafer cleaning in aqueous and organic systems*, Ph.D. dissertation, The University of Arizona (1993).

88. Leenaars, A. F. M., Huethorst, J. A. M., and van Oekel, J. J., *Langmuir*, 6(11):1701 (1990).

89. Lide, D. R., *CRC Handbook of Chemistry and Physics*, 90th Edition, p. 6–127, CRC Press, New York (2009–2010).